Aus dem Institut für Schlaganfall- und Demenzforschung (ISD)

Klinik der Universität München

Direktor: Prof. Dr. Martin Dichgans

Loss-of-function mechanisms
linked to HTRA1 Mac-domain mutations
causing cerebral small vessel disease

Dissertation

zum Erwerb des Doktorgrades der Medizin

an der Medizinischen Fakultät der

Ludwig–Maximilians–Universität zu München

vorgelegt von

Jonathan Alexander Johannes Gernert

aus Würzburg

2024

Mit Genehmigung der Medizinischen Fakultät

der Universität München

Berichterstatter:	Prof. Dr. Martin Dichgans
Mitberichterstatter:	PD Dr. Christof Haffner
	PD Dr. Lucia Gerstl
Mitbetreuung durch die promovierte Mitarbeiterin:	Dr. Nathalie Beaufort
Dekan:	Prof. Dr. med. Thomas Gudermann
Tag der mündlichen Prüfung:	07.03.2024

Eidesstattliche Versicherung

Ich erkläre hiermit an Eides statt, dass ich die vorliegende Dissertation mit dem Thema

Loss-of-function mechanisms linked to HTRA1 Mac-domain mutations causing cerebral small vessel disease

selbständig verfasst, mich außer der angegebenen keiner weiteren Hilfsmittel bedient und alle Erkenntnisse, die aus dem Schrifttum ganz oder annähernd übernommen sind, als solche kenntlich gemacht und nach ihrer Herkunft unter Bezeichnung der Fundstelle einzeln nachgewiesen habe. Ich erkläre des Weiteren, dass die hier vorgelegte Dissertation nicht in gleicher oder in ähnlicher Form bei einer anderen Stelle zur Erlangung eines akademischen Grades eingereicht wurde.

München, 08.04.2024   *Jonathan A. Gernert*

                                                         _____

                                                         Jonathan A. Gernert

Table of Contents

List of Abbreviations

A
aa   Amino acid
AHT   Arterial hypertension
AU   Arbitrary units

B
BCA   Bicinchoninic acid
BSA   Bovine serum albumin

C
CADASIL   Cerebral autosomal dominant arteriopathy with subcortical infarcts and leukoencephalopathy
CARASIL   Cerebral autosomal recessive arteriopathy with subcortical infarcts and leukoencephalopathy
CSVD   Cerebral small vessel disease

D
DMSO   Dimethyl sulfoxide
DNA   Deoxyribonucleic acid
DTT   Dithiothreitol

E
ECM   Extracellular matrix
EDTA   Ethylenediaminetetraacetic acid

F
FCS   Fetal calf serum
FL   Full-length
FLAIR   Fluid-attenuated inversion recovery (MRI sequence)

G
GWAS   Genome-wide association study

H
HEK-293T   Human embryonic kidney 293 cells
HTRA1   High-temperature requirement factor A1

I
ICH   Intracranial haemorrhage
IGFBP   Insulin-like growth factor binding protein

L
LB   Lysogeny broth
LTBP   Latent transforming growth factor β binding protein

M
MEF   Mouse embryonic fibroblast
MRI   Magnetic resonance imaging
mRNA   Messenger ribonucleic acid

P
PBS   Phosphate buffered saline
PCR   Polymerase chain reaction

R
RIPA   Radioimmunoprecipitation assay buffer

S
SDS-PAGE   Sodium dodecyl sulphate polyacrylamide gel electrophoresis
SNP   Single-nucleotide polymorphism

T
TGF-beta   Transforming growth factor -beta
TBS-T   Tris buffered saline with Tween 20

W

WT   Wild-type
WMH   White matter hyperintensities

List of Figures

List of Tables

1 - Abstract

Introduction. Mono- and biallelic mutations in the gene encoding the secreted serine protease high temperature requirement protein A1 (HTRA1) cause familial cerebral small vessel disease (CSVD) manifesting with ischemic stroke and dementia. Archetypal disease-causing mutations include nonsense and missense mutations that target the protease-domain of HTRA1 and impair its function. A set of missense mutations targeting the aminoterminal Mac-domain of HTRA1 have recently been identified in CSVD cases. The function of this domain has not been elucidated and the disease-related Mac-domain mutations leave HTRA1 proteolytically active *in vitro*.

Aims. The objectives of the present work were to examine the phenotype of CSVD cases carrying HTRA1 Mac-domain mutations and to study the consequences of these mutations on key molecular and cellular aspects of HTRA1 function.

Results. Based on a literature review, I determined that the phenotype of the seven reported Mac-domain mutation carriers recapitulates that of archetypal mutations carriers, although there is a trend towards a lower prevalence of stroke and non-neurological symptoms. Of interest, disease-related mutations are clustered in the Kazal-region of the Mac-domain. Biochemical analysis of HTRA1 protein stability in human cells transfected to overexpress recombinant HTRA1 indicated that one of the Mac-domain mutants (S121R) is rapidly degraded compared to control HTRA1. Moreover, analysis of purified proteins revealed that the conformation of this mutant is distinct from that of control HTRA1, thus suggesting partial misfolding of HTRA1-S121R. Protease activity measurements towards analytical as well as physiological substrates further demonstrated that the enzymatic activity of the Mac-domain mutants is comparable to that of HTRA1 wild-type. Exploring the interaction of HTRA1 with the extracellular matrix (ECM), I determined that the Mac-domain is involved in the insertion of HTRA1 in the ECM and identified vitronectin and fibronectin as putative ECM partners of HTRA1. However, I found that the ECM deposition of the Mac-domain mutants is comparable to that of control HTRA1.

Conclusion. Collectively, my work provides novel insights in the pathogenesis of HTRA1-related CSVD.

2 - Zusammenfassung

Einleitung. Mono- und biallelische Mutationen im Gen der sekretierten Serin Protease HTRA1 (high temperature requirement protein A1) verursachen eine familiär cerebrale Mikroangiopathie (CSVD), die sich mit ischämischen Schlaganfällen und Demenz manifestiert. Archetypische krankheitsverursachende HTRA1 Mutationen beinhalten Nonsense- und Missense-Mutationen, die auf die Protease-Domäne abzielen und ihre Funktion beeinträchtigen. Kürzlich wurde eine Reihe an Missense-Mutationen in CSVD-Fällen identifiziert, welche auf die aminoterminale Mac-Domäne abzielen. Die Funktion(en) dieser Domäne wurden bisher nicht geklärt und die krankheitsassoziierten Mac-Domäne Mutationen lassen HTRA1 *in vitro* proteolytisch aktiv.

Ziel. Ziel der vorliegenden Arbeit war es, den Phänotyp von CSVD-Fällen mit HTRA1 Mac-Domäne Mutationen und die Auswirkungen dieser Mutationen auf wichtige molekulare und zelluläre Aspekte der HTRA1-Funktion zu untersuchen.

Ergebnisse. Basierend auf einer Literaturübersicht stellte ich fest, dass der Phänotyp der sieben beschriebenen Mac-Domäne Mutationsträger den der archetypischen Mutationsträger widerspiegelt, wobei es einen Trend zu einer niedrigeren Prävalenz von Schlaganfällen und nicht-neurologischen Manifestationen gibt. Krankheitsassoziierte Mutationen gruppieren sich zudem in der Kazal-Region der Mac-Domäne. Biochemische Analysen der HTRA1 Protein Stabilität in humanen Zellen, transfiziert zur Überexpression von rekombinantem HTRA1, zeigten, dass eine Mac-Domäne Mutante (S121R) im Vergleich zum Kontroll-HTRA1 rasch abgebaut wird. Entsprechend ergab die Untersuchung aufgereinigter Proteine, dass sich die Konformation dieser Mutante von der des Kontroll-HTRA1 unterscheidet, was auf eine teilweise Fehlfaltung von HTRA1-S121R hinweist. Die Untersuchung der Protease Aktivität gegenüber analytischen und physiologischen Substraten demonstrierte, dass die enzymatische Aktivität von Mac-Domäne Mutanten vergleichbar mit dem HTRA1 Wildtyp ist. Schließlich untersuchte ich die Wechselwirkung von HTRA1 mit der extrazellulären Matrix (ECM): Ich stellte fest, dass die Mac-Domäne an der Insertion von HTRA1 in die ECM beteiligt ist und identifizierte Vitronectin und Fibronectin als mutmaßliche ECM-Partner von HTRA1. Die Ablagerung in der ECM der HTRA1 Mac-Domänen Mutanten scheint jedoch mit der von Kontroll-HTRA1 vergleichbar zu sein.

Fazit. Zusammenfassend liefert die Arbeit neue Einblicke in die Pathogenese der HTRA1-assoziierten CSVD.

3 - Introduction

3.1 - Cerebral small vessel disease

Cerebral small vessel disease (CSVD) is an array of disorders affecting cerebral small arteries, arterioles, and capillaries as well as veins and venules (**Figure 1A**). CSVD leads to brain damage in the white and deep grey matter and is associated with a broad spectrum of clinical manifestations [1, 2].

There are two main subtypes of CSVD: cerebral amyloid angiopathy and non-amyloid CSVD. My dissertation will focus on non-amyloid CSVD.
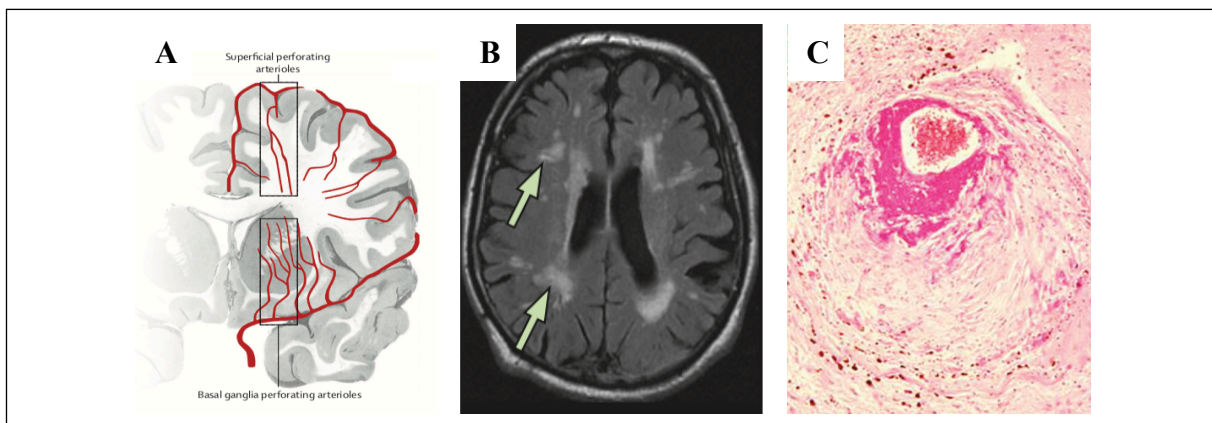
Figure 1: Hallmarks of CSVD.
A: Architecture of arterial cerebral vasculature (based on [2]). B: Neuroimaging finding in CSVD (arrows: white matter hyperintensities (WMH) on a fluid-attenuated inversion recovery (FLAIR) magnetic resonance imaging (MRI) sequence; based on [3]). C: Histopathological finding in CSVD (fibrinoid necrosis detected by hematoxylin and eosin staining, x20; based on [1]).

3.1.1 - Fundamentals of CSVD

Historically CSVD was clinicopathologically described by C. M. Fisher in the 1960s [4], then progressively developed with neuroimaging techniques [3, 5] and got an emerging field with recent genome wide association studies (GWAS) [6].

CSVD plays an important role in **age-related diseases** [7]. It contributes to nearly half of dementia cases [8] either alone or in combination with neurodegenerative pathologies such as Alzheimer`s disease [9]. Further, a quarter of ischemic strokes and most intracranial haemorrhage (ICH) are related to small vessel pathologies [10]. However, the frequency of clinical effects is highly dependent on the underlying etiopathology.

In addition to dementia and stroke, **common clinical manifestations** of CSVD include *e.g.*, gait disturbance [11], incontinence [12], cognitive impairment and depression [13]. Increased transition to disability [12] and mortality [13] are correlated with CSVD neuroimaging features.

CSVD involves **multiple aetiologies**. On one hand, demographic factors such as age, sex and ethnicity [14, 15] as well as additional risk factors, including arterial hypertension (AHT), smoking, diabetes or obstructive sleep apnoea are associated with CSVD [16]. These are mainly responsible for an arteriosclerotic pathology [1]. On the other hand, genetic factors also contribute to the development of CSVD.

The **pathogenesis** of CSVD involves an array of mechanisms that affect small vessel's structure and function, ultimately leading to parenchymal - including neuronal - damage. In particular, neuroimaging (**Figure 1B**), histopathology (**Figure 1C**) and/or proteomic analyses have linked CSVD to *e.g.*, loss of the blood brain barrier integrity, endothelial dysfunction, loss of mural cells, impaired cerebrovascular reactivity, perturbations of the cerebrovascular matrisome as well as astrogliosis and possibly systemic inflammation [2, 17].

So far, no blood or cerebrospinal fluid diagnostic biomarker is recommended in the clinic [18]. CSVD **diagnosis** is mainly based on neuroimaging criteria. In 2013, an international working group (STRIVE) summarized typical MRI features linked to CSVD [5]. The most prominent pathology is white matter hyperintensities (WMH, **Figure 1B**), while lacunes, subcortical infarcts, cerebral microbleeds, enlarged perivascular spaces and brain atrophy are also common [5]. Of note, CSVD-related neuroimaging findings are detected in 70 % of 65-year-old individuals and almost all 90-year-olds [19]. Their clinical manifestations depend on their size and location. Some abnormalities result in very subtle neurological symptoms or even remain clinically silent [20].

Treatments options with proven efficacy against most CSVD are missing. Patients' management is mainly limited to *e.g.*, primary prevention with reduction of risk factors such as AHT [21] or prevention of stroke recurrence using antiplatelet therapy [22].

3.1.2 - Monogenic CSVD

The large majority of CSVD cases are sporadic. However, with the advancement of imaging and genetic analyses, an increasing number of monogenic CSVD has been identified over the past two decades (**Table 1**, CARASIL and *HTRA1*-related CSVD are presented in detail in section 3.2).

Disease	Gene Locus	Gene	Year	Reference
Axenfeld-Rieger Syndrome	6p25 4q25	*FOXC1* *PITX2*	2014	[23]
CADASIL	19p13	*NOTCH3*	1993	[24]
CARASAL	20q13	*CTSA*	2016	[25]
CARASIL and *HTRA1*-related CSVD	10q26	*HTRA1*	2009 2015	[26] [27]

COL4-related CSVD
   PADMAL
   hMID
	13q34	*COL4A1, COL4A2*	2007
			2010, 2016
			2017
				[28]
				[29] [30]
				[31]

DADA2	20q11	*CERC1*	2014	[32]
Fabry disease	Xq22	*α-GLA*	1970, 1987	[33] [34]

HCHWA
   Dutch type
   Icelandic type
	21q21
	20p11
		APP
		CST3
			1982, 1990
			1978, 1986
				[35] [36]
				[37] [38]

Hereditary small vessel disease of the brain, SVDB	unreported	unreported	2006	[39]
Homocystinuria	21q22 1p36	*CBS* *MTHFR*	1988 1981	[40] [41]
Incontinentia pigmenti	Xq28	*NEMO*	2000	[42]
MELAS	15q26	Multiple mitochondrial DNA genes *POLG*	1984 2007	[43] [44]
RVCL-S HERNS, CRV, HRV, HAS	3p21	*TREX1*	2008	[45]
Sickle cell disease	11p15	*HBB*	1949	[46]

Table 1: Monogenic diseases affecting cerebral small vessels.
An excerpt of monogenic CSVD is listed in alphabetic order: CADASIL: cerebral autosomal dominant arteriopathy with subcortical infarcts and leukoencephalopathy; CARASAL: cathepsin-A-related arteriopathy with strokes and leukoencephalopathy; CARASIL: cerebral autosomal recessive arteriopathy with subcortical infarcts and leukoencephalopathy; *HTRA1*-related CSVD (see section 1.2); COL4: type IV collagen; PADMAL: pontine autosomal dominant microangiopathy and leukoencephalopathy; hMID: hereditary multi-infarct dementia (of the Swedish type); DADA2: deficiency of the enzyme ADA2 (adenosine deaminase 2); HCHWA: hereditary cerebral haemorrhage with amyloidosis; MELAS: mitochondrial encephalopathy, lactic acidosis and stroke-like episodes; RVCL-S: retinal vasculopathy with cerebral leukodystrophy and systemic manifestations; HERNS: hereditary endotheliopathy with retinopathy, nephropathy, and stroke; CRV: cerebroretinal vasculopathy; HRV: hereditary vascular retinopathy; HSA: hereditary systemic angiopathy.

Overall, hereditary CSVD recapitulate the main clinical, neuroimaging and histopathological hallmarks of sporadic CSVD. However, they exhibit an earlier age of onset and a higher frequency of neurological burden. Furthermore, most Mendelian CSVD are independent of classical vascular risk factors and present with a specific pattern of extraneurological manifestations [47].

These disorders are rare to very rare: the most frequent Mendelian CSVD are CADASIL (cerebral autosomal dominant arteriopathy with subcortical infarcts and leukoencephalopathy) and Fabry disease, affecting 2-4 per 100,000 individuals [48, 49]. Nevertheless, inherited CSVD have been an **instrumental model** to study CSVD-related pathomechanisms and identify new drug targets [50].

Of interest, GWAS recently identified various genetic factors involved in sporadic CSVD. Among these, common genetic variants (SNPs: single-nucleotide polymorphisms) in genes involved in Mendelian CSVD such as *COL4A1/2*, *NOTCH3* and *HTRA1* confer risk of *e.g.*, WMH or stroke, suggesting that deregulation of the corresponding proteins contributes to sporadic CSVD [51-53].

3.2 - *HTRA1*-related CSVD

The high temperature requirement protein A1 (HTRA1) serine protease (see detailed description in section 3.3) is encoded by the *HTRA1* gene located on 10q26.13 [54].

3.2.1 - CARASIL

In 2009, Hara et al. identified **biallelic mutations in *HTRA1*** as being causative for cerebral autosomal recessive arteriopathy with subcortical infarcts and leukoencephalopathy (CARASIL), a rare Mendelian CSVD initially described in the 1970s [26, 55] (**Figure 2A**).
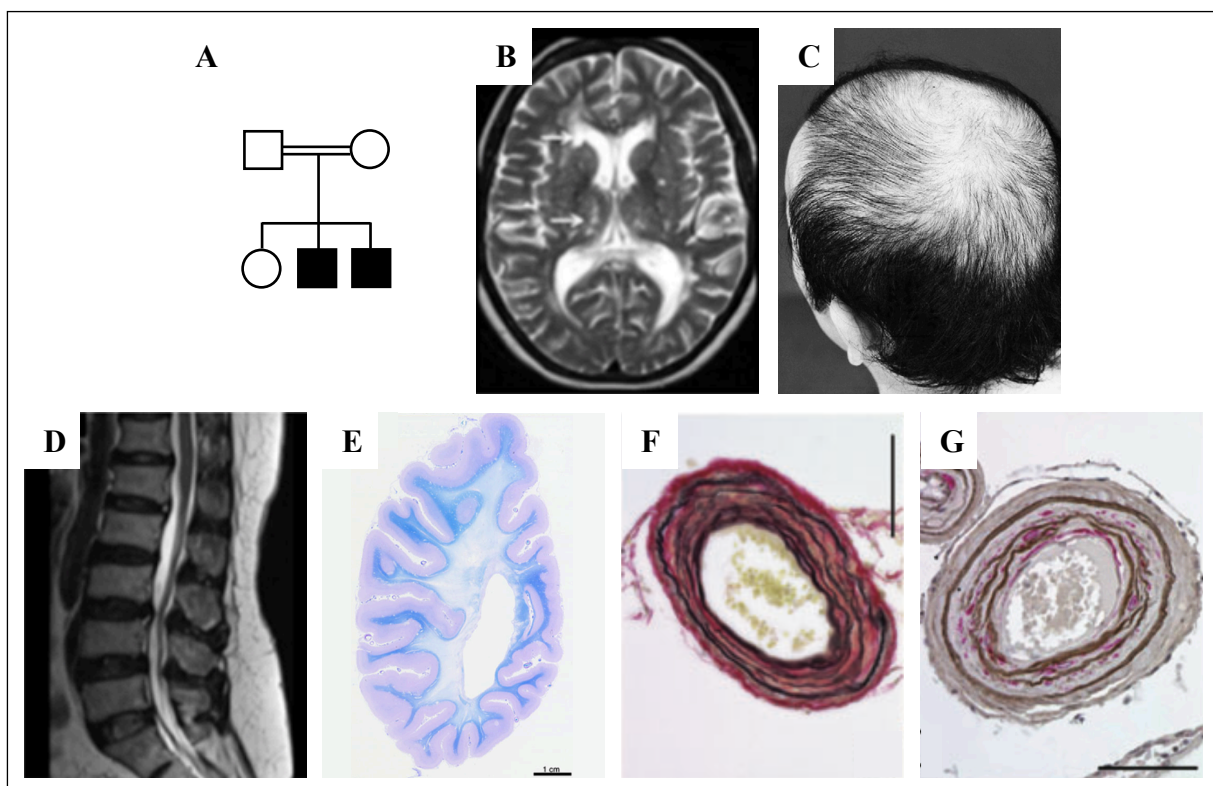
Figure 2: Main features in CARASIL cases.
A: Family tree of 2 homozygous, clinically affected CARASIL males (filled squares) with consanguine, clinically unaffected parents (double horizontal line) and their clinically unaffected daughter (open circle) (HTRA1 mutation V297M, based on [26]). B: Neuroimaging features of CARASIL patients include white matter and thalamic hyperintensities (T2-weigthed MRI, arrows; based on [56]). C: Alopecia (based on [57]) and D: spondylosis in a CARASIL case (T2-weigthed MRI; based on [56]). E: Demyelination (Luxol fast blue with haematoxylin and eosin staining; based on [58]). F: Small brain arteries exhibiting intimal thickening, splitting of the lamina elastica (Elastica von Gieson staining) and G: extensive loss of smooth muscle cells (anti-SMA (smooth muscle actin) staining, red) in a CARASIL brain vessel (F, G bars mark 100 μm; both based on [59]).

The **clinical phenotype** of CARASIL shows a unique pattern: On average, the disease manifests at 30 years of age [60] and leads to bed-ridden within 10 years, and death within 20-30 years [57]. In addition to WMH (**Figure 2B**), the main neurological symptoms include lacunar infarcts, cognitive impairment and gait disturbance [57, 60]. Seizures, depression,

migraine, or pseudobulbar paralysis are less common [60]. Besides, extraneurological features like young-onset alopecia (**Figure 2C**), spondylosis deformans (**Figure 2D**) and psychiatric disorders affects the majority of patients [18].

Histopathological examination of CARASIL brain reveals myelin loss (**Figure 2E**). The cerebral small vessels exhibit intimal thickening, splitting of the lamina elastica and smooth muscle cell loss (**Figure 2F**). Granular osmophilic material deposits, a hallmark of CADASIL, are absents [58, 61].

The **diagnosis** of CARASIL is based on the synopsis of clinical symptoms, positive family history, typical CSVD findings on neuroimaging and is verified by genetic testing [18]. To date, **no specific treatment** is available [18].

Over 50 CARASIL cases have been reported worldwide, mostly Asian [60]. In total 25 unique **homozygous or compound heterozygous mutations** have been identified (see section 3.4 for detailed description).

3.2.2 - Familial CSVD linked to heterozygous *HTRA1* mutations

In 2015, Verdura et al. published results from whole exome sequencing in families with a history of CSVD [27]. After exclusion of variants within known CSVD-genes, **heterozygous *HTRA1* mutations** were detected in about 5 % of the screened patients [27]. Further analysis of independent patient cohorts confirmed this princeps observation [62-65], thus highlighting *HTRA1* mutations as a significant aetiology in familial CSVD. In addition, several single cases have been identified. Within a short time period, the number of symptomatic patients carrying heterozygous *HTRA1* mutations has exceeded those of CARASIL, with over 60 patients and 39 known mutations [66]. Of note, the mutations partially overlap with mutations identified in CARASIL cases (see section 3.4).

Clinical manifestations in heterozygous *HTRA1* mutations carriers resemble those observed in CARASIL cases but differ by a later onset of symptoms (mean 54 years), a lower prevalence of gait disturbance and less if at all extraneurological symptoms [60]. Other remarkable differences include AHT, detected in up to 20 % cases, and a higher frequency of males [60]. Neuroimaging and histopathological examination of CARASIL and heterozygous mutation carriers show comparable features (**Figure 3**) [27].
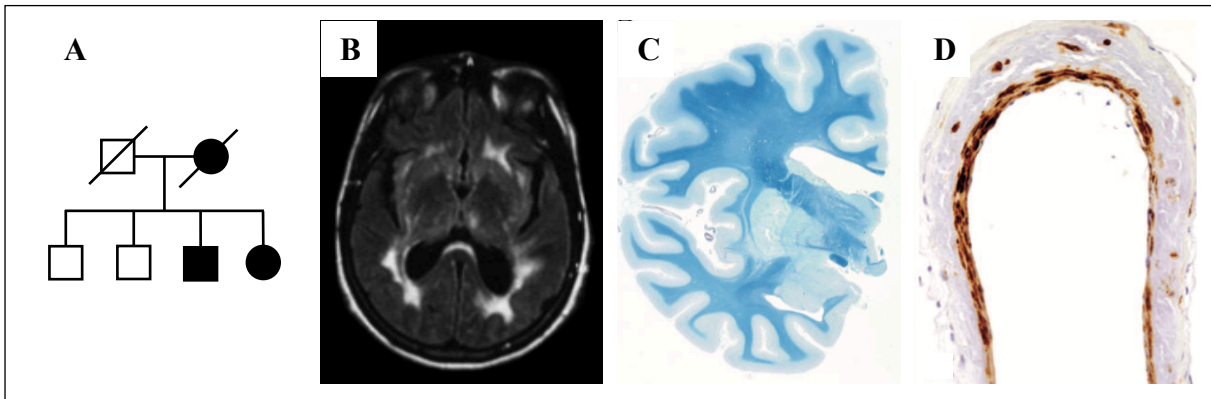
Figure 3: Main features in heterozygous *HTRA1* mutation carriers.
A: Family tree with 3 symptomatic individuals bearing heterozygous *HTRA1* mutation Q289X (filled symbols; squares represent men, circles women, open symbols are clinically unaffected, crossed out symbols are deceased individuals) (based on [64]). B: Neuroimaging of a heterozygous *HTRA1* mutation carrier reveals white matter hyperintensities (FLAIR; based on [27]). C: At a macroscopic level no major change is detected apart from cerebral atrophy (Luxol fast blue stain; based on [61]). D: Moderate loss of smooth muscle cells (anti-SMA staining; based on [61]).

CARASIL is a highly penetrant disorder. In contrast, **genotype/phenotype correlations are poorly understood in heterozygous mutation carriers**. While some individuals exhibit severe CSVD-related manifestations, others remain clinically asymptomatic or even display no remarkable neuroimaging abnormalities [60]. On one hand, combined with other vascular risk factors, *HTRA1* haploinsufficiency might suffice to cause late onset CSVD. On the other hand, a subset of mutations has been proposed to display dominant-negative properties (see section 3. 4).

3.2.3 - Common *HTRA1* variants linked to CSVD and stroke

Together with other Mendelian CSVD-associated genes *e.g.*, *COL4A1*, *COL4A2* and *NOTCH3*, common *HTRA1* variants were recently identified to be linked to CSVD and stroke [67, 68]. Specifically, the common *HTRA1* intronic variant rs2293871 (c.1275-36C>T frequency in 1,000 Genomes: C = 0.7388, T = 0.2612) is associated with altered gene expression in human brain tissue and extreme CSVD [69, 70]. In addition, SNPs within *HTRA1* reached a subthreshold level for all-type and small-vessel stroke in the MEGASTROKE-study [51]. Overall, these observations suggest that deregulation of HTRA1 expression contributes to sporadic CSVD and stroke.

3.3 - The HTRA1 protease

3.3.1 - HtrA proteases

HTRA1 belongs to the HtrA serine protease family that is highly conserved among species. In humans, 4 HtrA serine proteases are described: HTRA1-4. HTRA1, HTRA3 and HTRA4 are secreted enzymes, whereas HTRA2, which is lacking the aminoterminal Mac-domain (see below), is mitochondrial [71, 72].

3.3.2 - HTRA1 domain organization

HTRA1 comprises 480 amino acids (aa), displays a molecular mass of 51 kDa and is organised in 5 distinct functional domains (**Figure 4**) [71].
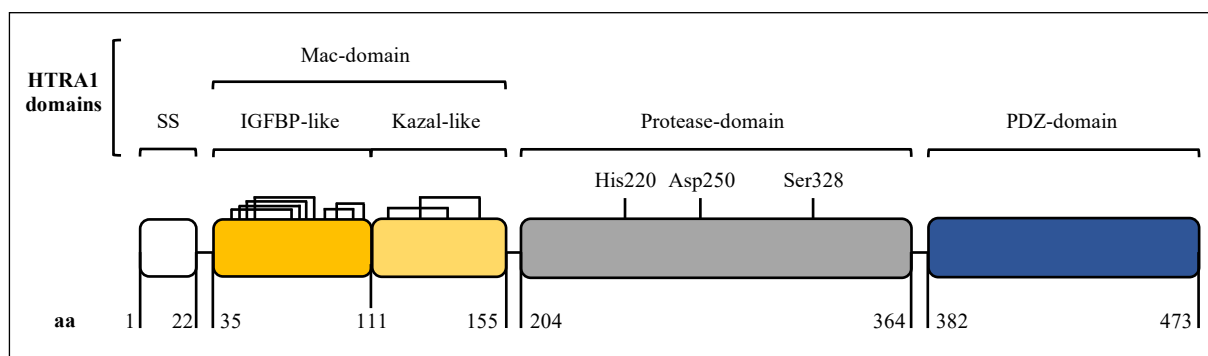
Figure 4: HTRA1 domain organization.
HTRA1 exhibits a signal peptide (SS), an aminoterminal Mac-domain composed of an IGFBP-like (insulin-lie growth factor binding protein) and a Kazal-like domain, a central serine protease-domain (catalytic residues: His^{220}, Asp^{250}, Ser^{328}) and a carboxyterminal PDZ-domain. The black lines mark the tight disulphide network within the Mac-domain. aa: amino acids. (Adapted from [73]).

Signal-peptide (Met^1 – Ala^{22})

HTRA1 bears a 22 aa signal-peptide composed of an aminoterminal basic region, a hydrophobic patch and a canonical site for cleavage by signal peptidase [74]. Accordingly, HTRA1 is a predominantly secreted enzyme.

Mac-domain (Ala^{35}– Cys^{155})

HTRA1 displays an aminoterminal Mac-domain composed of an Insulin-like growth factor-binding protein (IGFBP) -like and a Kazal-like domain. In addition to HTRA1, Mac-domains are restricted to only 5 other proteins: HTRA3, HTRA4, IGFBP7, IGFBP-like 1 and Kazal D1 [54, 75]. Their function, possibly related to protein-protein interactions, is not fully understood.

Autolysis of HTRA1 results in cleavage of the Mac-domain, a feature that is influenced by the redox stage [73]. In addition, truncated HTRA1 proteins lacking the Mac-domain have been detected *in vivo* [76, 77]. Therefore, HTRA1 Mac-domain has been speculated to display important regulatory functions [54]. However, the presence or absence of this domain was experimentally proved to leave HTRA1 protease activity unaffected [54].

IGFBP-like domain (Ala^{35} – Val^{111}): The aminoterminal region of the Mac-domain shares high sequence and structural homologies with IGF binding proteins, especially IGFBP4 [74, 78]. As in IGFBPs, the IGFBP-like domain of HTRA1 is stabilized by six cysteine bonds (**Figure 4**). However, its biological significance is unclear, as it neither binds IGF, nor influences HTRA1 protease activity [54].

Kazal-like domain (Ser^{115} – Cys^{155}): The carboxyterminal region of the Mac-domain shares sequence homology with Kazal-like domains, which are conserved protein domains usually indicative of serine protease inhibitors. However, compared to classical Kazal-domains, HTRA1 Kazal-like domain exhibits 2 instead of 3 disulphide bonds [54]. Accordingly, inhibition of HTRA1 itself or of other Kazal-sensitive proteases, including *e.g.*, trypsin and chymotrypsin was experimentally excluded (by comparison to α1-antitrypsin and aprotinin) [54].

Protease-domain (Gly^{204} – Leu^{364})
HTRA1 belongs to the protease clan P1, family S1. This evolutionarily conserved serine protease exhibits a trypsin-like protease-domain, including a catalytic triad with His^{220}, Asp^{250} and Ser^{328} [79]. The mechanisms that control the conversion from resting to active HTRA1 are described in the next paragraph.

PDZ-domain (Tyr^{382} – Val^{473})
HTRA1 displays a carboxyterminal PDZ-domain. PDZ-domains are generally involved in protein-protein interactions. In bacterial HtrAs, PDZ-domains are involved in oligomeric assembly and/or protease activation [80]. In contrast, the PDZ-domain of human HTRA1, neither impacts trimerization, nor influences protease activity [54, 81, 82].

3.3.3 - Structure and activation of HTRA1

As depicted in **Figure 5A**, HTRA1 is a homo-trimeric enzyme. The trimer displays a funnel-like shape: the catalytic domains are located within the trimer core, the PDZ-domains protrude to the outside, while the Mac-domains lie flat against the trimer side [54].

HTRA1 displays a unique, substrate-induced activation mechanism (**Figure 5B**). The substrate binds to the active site and interacts with the sensor loop L3. This induces an inter-protomer interaction of loop L3 with the activation loop LD, followed by a sequential positioning of loop L1 and L2, and of the catalytic site [72].

Importantly, since loop L3 and LD are exposed by adjacent monomers, the multimeric assembly of HTRA1 is mandatory for protease activity. Of note, both the trimeric and the active conformations are reversible.
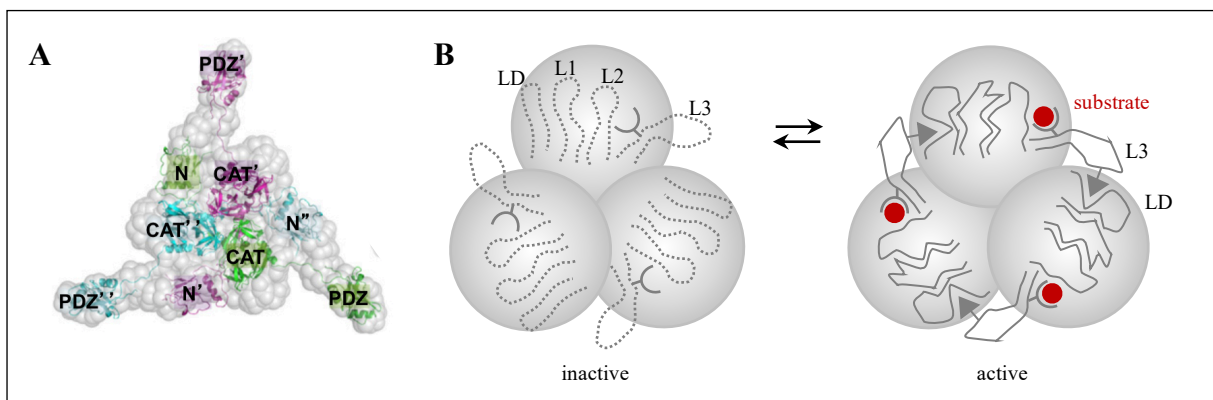
Figure 5: Structure and activation of HTRA1.
A: Structure of the HTRA1 trimer. HTRA1 domains are labeled: N (Mac-domain), CAT (protease-domain) and PDZ (PDZ-domain). Monomers are marked in blue, green and pink (based on [54]). B: Activation of trimeric HTRA1. HTRA1 activation cascade, which is initiated by substrate binding, involves large conformational rearrangements that require crosstalk between protomers. The loops are named based on chymotrypsin nomenclature (L1-3, LD; based on [82]).

3.3.4 - Localization, substrates, and functions of HTRA1

HTRA1 is expressed ubiquitously among human tissues. In the brain, it is mainly expressed by astrocytes, but it is also produced by all major vascular cell types (endothelial cells, smooth muscle cells, pericytes and fibroblasts) [83]. HTRA1 is localized in the extracellular space and associates with the extracellular matrix (ECM) [84, 85].

HTRA1 has been reported to target and cleave a plethora of substrates *in vitro*. These include membrane receptors and cell surface proteins (*e.g.*, TGF-beta receptor type-1 and -2

(transforming growth factor), Protein jagged-1, ADAM9 (disintegrin and metalloproteinase domain-containing protein 9)), growth factors and cytokines (TGF-beta, DKK3 (dikkopf-3); [86]) as well as matrisomal proteins (fibronectin, vitronectin, clusterin, fibulin 5, the TGF-beta ligands LTBP1 and 4 (latent-transforming growth factor beta binding protein)) [79] (LTBP4: not published). In accord with *in vitro* assays, the ECM and ECM-associated proteins listed above were found to accumulate in the brain vasculature of HTRA1-deficient mice [17]. Of note, apart from α1-antitrypsin and α1-macroglobulin, no natural HTRA1 inhibitor has been reported.

HTRA1 regulates cell signalling, proliferation, and survival. Accordingly, deregulation of HTRA1 accompanies and is assumed to be implicated in age-related macular degeneration [87, 88], pre-eclampsia [77], osteoarthritis and intervertebral disc degeneration [89], as well as various malignancies [90-92].

3.4 - *HTRA1* mutations linked to familial CSVD

Over 60 unique *HTRA1* mutations have been linked to familial CSVD (**Figure 6**). As a key pathomechanism, these mutations are assumed to impair HTRA1 protease function leading to an accumulation of HTRA1 substrates.

Disease-causing *HTRA1* mutations are typically nonsense, frameshift, or missense mutations [60]. Two **intronic mutations** have been reported in homozygous and/or heterozygous symptomatic carriers [27, 93]. Both are predicted to alter mRNA splicing.

A total of 15 different **nonsense and frameshift mutations** have been identified. Apart from R370X, pathogenic nonsense and frameshift HTRA1 mutations encode truncated proteins lacking one or more catalytic residues. HTRA1 R370X, which contains an intact catalytic triad, exhibits protease activity levels comparable to wild-type (WT) HTRA1 *in vitro* [69]. But the mutation was found to induce mRNA decay, thus reducing protein levels [69].

Missense mutations represent the majority of the pathogenic mutations. Most (*i.e.,* 34 out of 41) missense mutations target HTRA1 **protease-domain**. Several, but not all, have been identified both in homo- and heterozygous patients (**Figure 6**). *In vitro* biochemical assays have been performed for most protease-domain mutants, showing that they exhibit a moderate to strong reduction of protease activity [26, 27]. Further, it was demonstrated that a subset of mutations impairs the multimeric assembly of HTRA1 [62, 94]. It was subsequently proposed that mutations affecting HTRA1 trimerization or targeting loop L3 (residues 301-314) and LD (residues 283-291) display dominant-negative properties [62, 94].

Few disease-causing missense mutations targeting **non-protease domain** residues have also been identified. Specifically, heterozygous mutations have been detected in the Mac- (*i.e.*, G120D, S121R, A123S, R133G, S136G, Q151K) and PDZ-domains (D450H) of late onset CSVD cases. Some of the corresponding variants have been investigated *in vitro*, and were found to display no apparent loss of protease activity [94]. The underlying loss-of-function mechanism has not been elucidated so far.

SS	IGFBP-like	Kazal-like	Protease-domain			PDZ-domain

Biallelic mutations

Compound heterozygous mutations

E42fs - A321T
D320N - - G341R
R166H[#] - - G276fs[#]

Nonsense, frameshift and intronic mutations

SS/IGFBP-like	Protease-domain		
G56fs	K168X, E247fs, S270fs, E277fs	G283X	**R302X**, S328X, 1005+1G>T, R370X

Missense mutations

Kazal-like	Protease		PDZ
R166C, A173T	G206R, A252T, R274Q	**P285L**, **G295R**, **V297M**	L364P

Monoallelic mutations

Nonsense, frameshift and intronic mutations

IGFBP-like	Kazal-like	Protease-domain		
Q151X	A182fs	R197X, E277fs	Q289X	973-1G>A, **R302X**

Missense mutations

IGFBP-like	Kazal-like	Protease-domain			PDZ-domain
G120D, S121R, A123S, R133G, S136G, Q151K	**R166C**, L, A173P, V175M, V176A, I179N, H185R[#]	S205C, G206E, V216M, I256T, G276A	G283E, R, S284G, R, **P285L**, Q, F286V, **G295R**, **V297M**	R302Q, T319I, N324S, T	D450H

Figure 6: Pathogenic mono- and biallelic *HTRA1* mutations identified in symptomatic CSVD cases.
Reported mutations are classified as compound heterozygous (for biallelic mutations only), nonsense, frameshift and intronic mutations, or missense mutations. Mutations identified in both homo- and heterozygous mutation carriers are highlighted in bold. IGFBP: insulin-like growth factor binding protein; SS: signale peptide; #: unpublished cases.

4 - Aims of the dissertation

Recently, an increasing number of heterogeneous mutations within the Mac-domain of HTRA1 have been identified, that do not interfere with the apparent enzymatic activity of HTRA1 *in vitro*. In this context, the **aims of this dissertation** were:

    (i)   to evaluate the phenotype of Mac-domain mutation carriers,

    (ii)   to characterize the corresponding mutant proteins, and

    (iii)   to investigate putative loss-of-function mechanisms.

To these ends, I combined literature-based analysis of patients' characteristics, *in silico* analysis of the mutation's characteristics, and *in vitro* and *ex vivo* analysis of protein expression, stability, secretion, conformation, activity towards analytical and physiological substrates, and interaction with the ECM.

5 - Material and Methods

5.1 - Literature-based analysis of *HTRA1* mutation carriers

Literature-based analysis of monoallelic *HTRA1* mutation carriers was performed based on the PRISMA guidelines.

Search strategy. The search terms "CARASIL", "HTRA1 SVD" and "HTRA1 mutation" were reviewed on PubMed. Additionally, references of the articles and reviews were screened for additional *HTRA1* mutations. The period of publication dates was set from 2009, corresponding to the first description of mutations in *HTRA1* linked to CSVD [26], to end of December 2020.

Inclusion and exclusion criteria. Articles in English, German and French were included. In a first step, all types of reports were included which confirmed at least one monoallelic *HTRA1* mutation by genotyping. Relatives of the afflicted individual were included if the same *HTRA1* mutation was genetically verified. In a second step, neurologically asymptomatic cases were excluded. Neurological manifestations such as stroke, migraine, seizures, cognitive impairment, dementia, or gait disturbance were considered. In the following, alopecia and spondylosis were evaluated as typical extraneurological manifestations; psychiatric manifestations were also listed but not considered in the analysis.

Classification of *HTRA1* mutations. Mutations were classified as missense Mac-domain mutations or as archetypal *HTRA1* mutations. Archetypal *HTRA1* mutations consist of *(i)* nonsense or frameshift mutations resulting in the loss of at least one catalytic residue and *(ii)* missense mutations targeting the protease-domain. One intronic mutation (973-1G>A) and one missense mutation targeting the PDZ-domain (D450H) were excluded.

Summary of patient data. If available, patient demographic, clinical and neuroimaging information was obtained from the literature.

5.2 - *In silico* analysis of missense Mac-domain mutations

Mutation prevalence. Following databases were used to evaluate the frequency of Mac-domain mutations: 1000 Genome frequency (Ensembl release 105) [1] [95], dbSNP [2] [96], ExAc (v1.0) [3] [97], gnomAD (v3.1.2) [4] [98, 99] and TOPMed (TOPMED Freeze 8, GRCh38) [5] [100].

Predicted pathogenicity. Pathogenicity was predicted using following *in silico* tools: PolyPhen2 [6] [101], SIFT [7] [102], Mutation Taster [8] [103], PROVEAN [9] [104] and Mutations Assessor [10] [105].

---

[1] http://www.ensembl.org/Homo_sapiens/Transcript/ProtVariations?db=core;g=ENSG00000166033;r=10:122458551-122514894;t=ENST00000368984; (accessed March 09, 2022)

[2] https://www.ncbi.nlm.nih.gov/variation/view/?term=htra1; (accessed March 09, 2022)

[3] https://gnomad.broadinstitute.org/gene/ENSG00000166033?dataset=exac; (accessed March 09, 2022)

[4] https://gnomad.broadinstitute.org/gene/ENSG00000166033?dataset=gnomad_r3; (accessed March 09, 2022)

[5] https://bravo.sph.umich.edu/freeze8/hg38/gene/snv/HTRA1; (accessed March 09, 2022)

[6] http://genetics.bwh.harvard.edu/pph2/index.shtml; (accessed March 09, 2022)

[7] https://sift.bii.a-star.edu.sg; (accessed January 01, 2021)

[8] https://www.mutationtaster.org; (accessed February 01, 2021)

[9] http://provean.jcvi.org/seq_submit.php; (accessed February 01, 2021)

[10] http://mutationassessor.org/r3/; (accessed January 31, 2021)

5.3 - Eukaryotic cell expression vectors

5.3.1 - Expression vectors provided by my host laboratory

Full-length HTRA1 constructs. pcDNA4/TO/Myc-His and pcDNA6/V5-His vectors encoding the cDNA of full-length (FL) human HTRA1 (aa 1-480) either WT, bearing an active site mutation (S328A) or bearing various disease-related mutations were used.

Truncated HTRA1 constructs. A Peak-12 vector encoding a CD5 signal peptide an amino-terminal HA tag, the cDNA of a truncated form of human HTRA1 lacking the Mac-domain (ΔMac-HTRA1, aa 158-480) and a carboxy-terminal V5-His tag, a pcDNA6/V5-His vector encoding the cDNA of a truncated form of human HTRA1 lacking the PDZ-domain (ΔPDZ-HTRA1, aa 1-371) and a Peak-12 vector encoding a CD5 signal peptide, an amino-terminal HA tag, the cDNA of the catalytic domain of human HTRA1 (Cat-HTRA1, lacking both the Mac- and the PDZ-domain, aa 158-371) and a carboxy-terminal V5-His were used.

Other expression vectors. A pcDNA6/V5-His vector (Thermo Fisher Scientific) and a pTT5 vector encoding the cDNA of the amino-terminal region of human LTBP1 (aa 1-689) fused to a carboxy-terminal V5-His tag were used.

5.3.2 - Cloning of expression vectors

All cloned constructs are listed in **Table 2**.

Construct	HTRA1 sequence (aa)	Mutation(s)	Tags	Construct used as template to generate the insert	PCR primers*	Construct used to generate the vector	Restriction enzymes and buffer	Insert size	Vector size	New construct size
HTRA1 S121R S328A	1-480	S121R S328A	C$_t$: Myc-His	HTRA1-S121R-Myc-His	NA	HTRA1-*S328A*-*Myc-His*	EcoRI and BstEII (NEB Cutsmart)	1.5 kb	5.0 kb	6.5 kb
HTRA1 A123S S328A	1-480	A123S S328A	C$_t$: Myc-His	HTRA1-A123S-Myc-His	NA	HTRA1-*S328A*-*Myc-His*	EcoRI and BstEII (NEB Cutsmart)	1.5 kb	5.0 kb	6.5 kb
HTRA1 R133G S328A	1-480	R133G S328A	C$_t$: Myc-His	HTRA1-R133G-Myc-His	NA	HTRA1-*S328A*-*Myc-His*	EcoRI and BstEII (NEB Cutsmart)	1.5 kb	5.0 kb	6.5 kb
ΔMac-HTRA1 S328A	158-480	S328A	N$_t$: HA C$_t$: V5-His	HTRA1-S328A-Myc-His	F: GATCTAGAAGGGCAGGAAGATCCCAA R: GATCTAGATGGGTCAATTTCTTCGGG	HA-LTBP1-*V5-His*	XbaI (NEB 2.1)	1.0 kb	7.1 kb	8.1 kb
ΔPDZ-HTRA1 S328A	1-371	S328A	C$_t$: V5-His	HTRA1-S328A-Myc-His	F: GATCTAGACAGTGTGGTGGAATTCGT R: GATCTAGATTTTCCTTTGGCCTGTCG	pcDNA6-*V5-His*	XbaI (NEB 2.1)	1.0 kb	5.0 kb	6.0 kb
Mac-domain	1-168	NA	C$_t$: V5-His	HTRA1-S328A-Myc-His	F: GATCTAGACAGTGTGGTGGAATTCGT R: GATCTAGATTGGGATCTTCCTGCCCT	pcDNA6-*V5-His*	XbaI (NEB 2.1)	0.5 kb	5.0 kb	5.5 kb
Mac-domain S121R	1-168	S121R	C$_t$: V5-His	HTRA1-S121R-Myc-His	F: GATCTAGACAGTGTGGTGGAATTCGT R: GATCTAGATTGGGATCTTCCTGCCCT	pcDNA6-*V5-His*	XbaI (NEB 2.1)	0.5 kb	5.0 kb	5.5 kb
Mac-domain A123S	1-168	A123S	C$_t$: V5-His	HTRA1-A123S-Myc-His	F: GATCTAGACAGTGTGGTGGAATTCGT R: GATCTAGATTGGGATCTTCCTGCCCT	pcDNA6-*V5-His*	XbaI (NEB 2.1)	0.5 kb	5.0 kb	5.5 kb
Mac-domain R133G	1-168	R133G	C$_t$: V5-His	HTRA1-R133G-Myc-His	F: GATCTAGACAGTGTGGTGGAATTCGT R: GATCTAGATTGGGATCTTCCTGCCCT	pcDNA6-*V5-His*	XbaI (NEB 2.1)	0.5 kb	5.0 kb	5.5 kb
Protease-domain S328A	158-371	S328A	N$_t$: HA C$_t$: V5-His	HTRA1-S328A-Myc-His	F: GATCTAGAAGGGCAGGAAGATCCCAA R: GATCTAGATTTTCCTTTGGCCTGTCG	HA-LTBP1-*V5-His*	XbaI (NEB 2.1)	0.6 kb	7.1 kb	7.7 kb
PDZ-domain	364-480	NA	N$_t$: HA C$_t$: V5-His	HTRA1-S328A-Myc-His	F: GATCTAGAAAAGTTCCTCACGGAGTC R: GATCTAGATGGGTCAATTTCTTCGGG	HA-LTBP1-*V5-His*	XbaI (NEB 2.1)	0.35 kb	7.1 kb	7.5 kb

Table 2: Generation of new expression vectors.
*Primers were designed using the CLC Main Workbench software (Qiagen) and were ordered from Metabion. They display a short 5′ extension, a restriction site (underlined) and the complementary sequence of the target cDNA. aa: amino acid; C$_t$: carboxy-terminal; kb: kilo base; NA: not applicable; N$_t$: amino-terminal; PCR: polymerase chain reaction.

5.3.2.1 - Synthesis of the inserts by PCR

When indicated, the insert was generated by PCR (polymerase chain reaction) using the cDNA template and primers listed in **Table 2**. The PCR mix contained 150 ng cDNA, 300-400 nM of forward and reverse primers and 1 µl of Accu Prime polymerase (Qiagen) with corresponding buffer A (Qiagen, containing dNTPs (nucleoside triphosphate)) in a final volume of 50 µl. Alternatively, 1 µl of *Pfu* polymerase (Stratagene) prepared in the buffer supplied by the manufacturer and 1 µl dNTPs (GE Healthcare) were used.

PCR was conducted on a peqSTAR Thermocycler (VWR Peqlab) using following program:

Procedure	Time	Temperature	Cycles
Denaturation	5 min	95°C	1
Denaturation	30 sec	95°C	
Annealing	30 sec	55°C	35
Elongation	2 min	72°C	
Elongation	10 min	72°C	1
Storage	Infinite	4°C	

5.3.2.2 - Purification of the PCR amplicons

Amplicons were purified using a PCR Purification kit (Roche): binding buffer was added to the PCR mix and samples were loaded on a small column containing a silica membrane. After centrifugation for 30 sec at 11,000 g and washing, DNA was eluted with 30 µl elution buffer and quantified using a Nanodrop spectrophotometer (ND-1000 by Thermo Fisher Scientific).

5.3.2.3 - cDNA digestion by restriction enzymes

Inserts were derived from the PCR amplicons or from an available plasmid, vectors were derived from an available plasmid (**Table 2**). 1 µg cDNA was incubated in the presence of 5-20 U restriction enzyme and of the appropriate restriction buffer (**Table 2**, enzymes, and restriction buffers all from New England Biolab) in a final volume of 25 µl for 1 h 30 min at 37°C.

5.3.2.4 - Vector dephosphorylation

To avoid auto-ligation, the vector was added with 1 µl antarctic alkaline phosphatase (New England Biolabs) and its corresponding alkaline phosphatase buffer and was incubated for 1 h at 37°C.

5.3.2.5 - DNA electrophoresis

10 µl of insert or vector were added with loading buffer (New England Biolabs) and subjected to gel electrophoresis. Gels contained 1 % (w/v) agarose prepared in 1x TAE buffer (Carl Roth) and were added with 1:100,000 SYBR safe (Invitrogen). 5 µl of PeqGold DNA ladder (100-10,000 base pair; VWR Peqlab) were included in each run as standard. Electrophoresis was performed within Perfect blue gel system devices (VWR Peqlab) filled with TAE buffer at 80 V for 1 h. DNA was visualized on an UV table (ultraviolet; Vilber-Lourmat).

5.3.2.6 - DNA gel extraction

Gel pieces containing the DNA fragment of interest were cut and the DNA was retrieved using the GeneJet DNA extraction kit (Thermoscientific). First, 100 µl binding buffer were added per mg gel. Second, samples were heated for 10 min at 55°C to melt agarose, then loaded on a silica membrane. After washing, DNA was eluted with 25 µl H_2O and quantified using a Nanodrop spectrophotometer.

5.3.2.7 - DNA ligation

50 ng vector were mixed with the insert in a molecular ratio of 1:3 in the presence of 1 µl T4 DNA ligase (New England Biolabs) and its corresponding DNA ligase buffer in a final volume of 15 µl at room temperature for 1 h. An insert-free sample was prepared as negative control.

5.3.2.8 - Bacterial transformation

Competent Escherichia coli DH5α bacteria (50 µl in-house prepared suspension) were thawed on ice and added with 2 µl ligation mix. After 30 min at 4°C, bacteria were heat shocked at 42°C for 90 sec, then cooled on ice for 2 min. 50 µl LB medium (lysogeny broth; the composition of the different buffer solutions is provided in **Table 3**) were added and the bacteria were kept at 37°C for 30 min. This mix was seeded on LB-agar plates containing a selection antibiotic (*i.e.*, 0.1 mg/ml ampicillin, as all plasmids encoded an ampicillin-resistance gene). The plates were incubated overnight at 37°C.

Solution	Composition	
Colloidal Coomassie staining solution	0.02 % (w/v)	Coomassie Brilliant Blue R
	5 % (w/v)	Aluminium sulfate hydrate
	2 % (v/v)	o-phosphoric acid
	10 % (v/v)	Ethanol
Laemmli buffer 5x (pH 6.8)	375 mM	Tris-base
	30 % (v/v)	Glycerol
	6 % (w/v)	Sodium dodecyl sulfate (SDS)
	500 mM	Dithiothreitol (DTT)
	0.03 % (w/v)	Bromophenol Blue
LB agar (pH 7.0)	5 g/l	Yeast extract
	10 g/l	Peptone
	5 g/l	NaCl
	1.5 %	Agar-Agar
LB medium (pH 7.0)	5 g/l	Yeast extract
	10 g/l	Peptone
	5 g/l	NaCl
Protein electrophoresis buffer (pH 8.3)	25 mM	Tris-base
	192 mM	Glycine
	0.1 % (w/v)	SDS
Protein transfer buffer (pH 8.3)	25 mM	Tris-base
	192 mM	Glycine
	20 % (v/v)	Methanol
RIPA buffer (pH 7.2)	50 mM	Tris
	150 mM	NaCl
	1% (v/v)	Triton-X 100
	1% (w/v)	Sodium deoxycholate
	0.5 % (w/v)	SDS
TBS-T (pH 8.0)	10 mM	Tris-base
	150 mM	NaCl
	0.05 % (v/v)	Tween 20

Table 3: Composition of buffers and solutions.
Reagents are listed by alphabetic order. LB: lysogeny broth; RIPA: radioimmunoprecipitation assay; TBS-T Tris buffered saline with Tween 20.

5.3.2.9 - Bacterial growth

Single bacterial colonies were transferred from LB-agar into liquid LB containing 0.1 mg/ml ampicillin using a sterile cloning circle. For small cultures, 2 ml medium were prepared in 5 ml round bottom tubes. For large cultures, 100 ml medium were prepared in 250 ml Erlenmeyer flask. Bacteria were grown for 8-15 h at 37°C and 225 rpm in an orbital shaker (Statorius Stedim Biotech).

5.3.2.10 - Purification of plasmidic DNA

The NucleoSpin Plasmid kit was used for small cultures and the NucleoBond Xtra Midi kit was used for large cultures to extract plasmidic DNA (both Macherey-Nagel). After cell resuspension in a RNase-containing solution followed by cell lysis, the lysis buffer was neutralized, and samples were centrifuged to remove debris. DNA was bound to a silica membrane, washed, and eluted by addition of 25 µl up to 5 ml of elution buffer. The DNA retrieved from large cultures was further precipitated with isopropanol, the pellet was washed with ethanol and resuspended in dH_2O. The amount of DNA was measured using a Nanodrop spectrophotometer, as described above. Samples were stored at -20°C until use.

5.3.2.11 - Analysis of plasmidic DNA

Plasmids were treated with the restriction enzyme(s) used for cloning (**Table 2**) followed by agarose gel electrophoresis to select insert-containing constructs. The entire *HTRA1* cDNA was then sequenced (SupremeRun, GATC Biotech) to confirm the presence of the expected mutation(s) and verify the absence of off-targets.

5.4 - Cell-based experiments

5.4.1 - Cells

HEK-293T cells. HEK-293T cells (human embryonic kidney 293 cells; American type Culture Collection) are immortalized human embryonic kidney cells transformed with stable expression of SV40 large T antigen. These are easy to grow and transfect and are commonly used for overexpression of recombinant proteins.

Mouse embryonic fibroblasts. Fibroblasts (MEF) from 12.5 days pc *HTRA1$^{+/+}$* or *HTRA1$^{-/-}$* embryos were generated and immortalized by serial passaging by Eva Scharrer (ISD, Munich).

5.4.2 - Cell culture conditions

5.4.2.1 - General culture conditions

Cells were manipulated under sterile conditions in a vertical laminar flow hoot (Herasafe KS, Thermo Fisher Scientific). Cells were grown in a humidified atmosphere, at 37°C and 5 % (v/v) CO_2 (Binder 9040-0038). Culture medium was composed of Dulbecco´s modified Eagle´s medium (DMEM) added with GlutaMAX, 10 % (v/v) fetal calf serum (FCS), 100 µg/ml streptomycin, 100 U/ml penicillin as well as sodium pyruvate and 4.5 g/l D-glucose (all from Gibco-Invitrogen).

5.4.2.2 - Cell splitting and seeding

Cells were washed with phosphate buffer saline (PBS, Apotheke Klinikum der Universität München), then incubated with 0.25 % (w/v) trypsin/Ethylenediaminetetraacetic acid (Trypsin/EDTA, Gibco-Invitrogen) at room temperature until detachment. The suspension was added with fresh culture medium to neutralize the effect of Trypsin/EDTA, and cells were seeded in a culture flask or plate containing fresh medium. Dilution ranged from 1:5 to 1:10, depending on their proliferation. A Neubauer chamber was used to count detached cells, while cell concentration was determined as follows:

Cells per ml = counted cells within the chamber / 9 x 10,000.

The different types of culture plates and flasks (from Costar, Corning, Thermo Fisher Scientific or Nunc) with the corresponding reagent volumes or quantities are listed in **Table 4**.

	P96 well	P48 well	P24 well	P6 well	T25 flask	T80 flask	T175 triple flask
Size (cm^2)	0.32	0.84	2	9.5	25	80	175
PBS (ml)	0.1 - 0.2	0.5	0.5 - 1	1 - 2	2 - 5	5 - 10	40
Trypsin/EDTA (ml)	NA	NA	NA	2 drops	1	2	NA
Culture medium (ml)	0.1-0.2	0.5	0.5 - 1	1-2	5	10	90
OptiMEM (µl)	NA	NA	50	100	NA	NA	NA
Lipofectamin 2000 (µl)	NA	NA	0.75	1.5	NA	NA	NA
Plasmidic DNA (µg)	NA	NA	0.250	1.000	NA	NA	NA
Lysis buffer (ml)	NA	NA	0.010	0.015	0.5	1.0	NA

Table 4: Volume or quantities of cell culture reagents used in the different culture plates and flasks.
EDTA: ethylenediaminetetraacetic acid; NA: not applicable; OptiMEM: opti minimal essential medium; PBS: phosphate buffered saline.

5.4.2.3 - Cell freezing and defreezing

After detachment as described, the cells were pelleted at 400 *g* for 10 min, then resuspended in FCS containing 20 % (v/v) Dimethyl sulfoxide (DMSO; Sigma-Aldrich). Cell suspensions were transferred to cryotubes (2 tubes per T80 flask) and were cooled from 4°C to -80°C in a cryo-box filled with isopropanol. After 1-3 days, cells were stored in liquid nitrogen at -196°C. Cells were thawed to 37°C and seeded in a T80 flask with new culture medium. After adhesion, the medium was renewed to remove residual DMSO.

5.4.3 - Cell Transfection and treatment

5.4.3.1 - Transfection

Transient transfection. Lipofectamine 2000 (Invitrogen) was diluted in Opti Minimal Essential Medium (OptiMEM; reduced serum medium buffered with HEPES and sodium bicarbonate)/GlutaMAX (Gibco-Invitrogen) in a 3:50 ratio and incubated at room temperature for 5 min. Plasmidic DNA was diluted in OptiMEM. Lipofectamine and DNA were mixed at a 1.5 µl Lipofactamine / µg DNA ratio and incubated at room temperature for 15 min. 50-80 % confluent cell layers were washed with phosphate buffered saline (PBS), added with fresh medium and the Lipofectamine / DNA mix was added drop by drop to the culture medium. Transfected cells were maintained in culture for 24-72 h.

Selection of stably transfected cells. To achieve stable transfection, cells were detached 48 h post-transfection and were seeded in new culture plates at serial dilutions ranging from 1:3 to

1:243 in culture medium containing 100 µg/ml Zeocin as a selection antibiotic (Invitrogen). Selection pressure was maintained for 2 weeks. Non-transfected cells were used as negative control.

5.4.3.2 - Assay-specific culture conditions

HTRA1 secretion, purification, and protease activity measurements. For all experiments performed under FCS-free conditions, cells were seeded on plasticware coated with 0.01 % poly-L lysin (Sigma Aldrich) for 5 min at room temperature to minimize anoikis.

Cycloheximide chase. 24 h post-transfection, cells were exposed to complete medium added with 0.05 mg/ml of the translation inhibitor cycloheximide (Sigma-Aldrich) and kept in culture for 0.5 h, 1.5 h, 5 h. Cycloheximide-free wells with 0.05 % DMSO (Sigma-Aldrich) were prepared at t = 0 h as baseline.

5.4.4 - Collection and preparation of cell extracts

5.4.4.1 - Collection of cell culture medium

FCS-free cell secretomes were collected, centrifuged for 10 min at 400 g to remove debris and stored at -20°C.

5.4.4.2 - Cell Lysis

RIPA buffer lysis. After washing with PBS, cells were lysed for 20 min at 4 °C using RIPA (radioimmunoprecipitation assay) buffer added with commercial cocktails of protease and phosphatase inhibitors (Roche). Insoluble material was removed by centrifugation for 10 min at 11,000 g and samples were stored at -20°C.

Triton/NH₃ buffer lysis. When the ECM was to be retrieved from fibroblast cultures (see below), a buffer made of 0.1 % (v/v) Triton X-100 and 20 mM NH_3 in PBS was applied for 20 min at room temperature to lyse cells. The cell lysate was centrifuged for 10 min at 11,000 g and stored at -20°C.

5.4.4.3 - ECM retrieval

Following cell lysis with Triton/NH₃ buffer (see above), wells were washed with PBS added with 10 mM Tris, 150 mM NaCl, 0.5 % (w/v) sodium deoxycholate then in PBS added with 2 mM Tris pH 8.0. ECM proteins were recovered by solubilization in Laemmli buffer for 10 min at 80°C. Samples were collected and stored at -20°C.

5.5 - HTRA1 purification

HEK-293T cells stably transfected to overexpress HTRA1 were seeded in poly-L-lysin coated triple flask (usually 4 flasks per assay), grown to confluence, washed twice with PBS and FCS-starved for 4 to 5 days. Dialysis bags (Dialysierschlauch Visking Cellulose, Typ 27/32 inch; wall thickness 0,023 mm; B 34 mm) were heated at 70°C for 30 min in buffer containing 1 mM EDTA and 2 % (w/v) sodium bicarbonate, then stored in dH_2O at 4°C. Culture medium was collected, centrifuged 10 min at 400 g, and dialysed for 2 h at room temperature against 0.5x PBS, then for 12 h at 4°C against 0.5x PBS added with 200 mM NaCl. Culture medium was added with Superflow Talon resin (Clontech). This His-tagged protein binding resin consists of agarose beads crosslinked with an immobilized chelating group precharged with Co^{2+} ions. The mix was gently agitated for 1 h at room temperature and following centrifugation for 10 min at 700 g, the resin was transferred on a disposable gravity column (Clontech). After sequential washings with 10 ml washing buffer (6 mM sodium phosphate, 100 mM NaCl, pH 7.0), 2 x 10 ml washing buffer supplemented with 0.5 % (w/v) imidazole, and 10 ml washing buffer, bound proteins were eluted with 4 ml PBS containing 100 mM EDTA. 250 µl fractions were collected and analysed by SDS-PAGE and Coomassie staining (see below). The three fractions containing the highest concentration of recombinant HTRA1 (usually in the range 0.2-1 mg/ml) were pooled and dialyzed overnight against 5,000 volumes of 50 mM Tris, 500 mM NaCl pH 8.0 or PBS buffer. When required, the medium was centrifuged in a 10 kDa cut-off Amicon filter (Millipore) at 3,000 g to reach an HTRA1 concentration $\geq$ 0.2 mg/ml.

5.6 - Protein analysis

5.6.1 - Measurement of protein concentration

The Pierce bicinchoninic acid (BCA) assay kit (Thermo Fisher Scientific) was used to measure total protein concentration. 10 µl sample or bovine serum albumin (BSA, BioRad) diluted to 0.0125-2 mg/ml as standard were added with 75 µl BCA solution (in a buffer A:B ratio of 50:1) and incubated at 37°C for 20 min. The absorbance at 595 nm was measured on an iMark microplate reader (Biorad) and the BSA standard curve was used to extrapolate sample protein concentration.

5.6.2 - Analysis of HTRA1 conformation

Limited digestion by trypsin. To evaluate protein conformation, purified recombinant HTRA1 was diluted to 0.5 µM in PBS and exposed to 100 nM trypsin (Invitrogen) for increasing time periods at 37°C. A trypsin-free sample served as control. HTRA1 processing was analyzed by SDS-PAGE followed by Coomassie staining as described below.

Glutaraldehyde-based crosslinking. To determine the oligomeric state of HTRA1, purified recombinant HTRA1 was diluted to 0.5 µM in 50 mM HEPES (4-(2-hydroxyethyl)-1-piperazineethanesulfonic acid), 120 mM NaCl pH 7.5 and was incubated at 37°C for 5 min with shaking at 300 rpm. Upon addition of glutaraldehyde (0.5 % (v/v)) the mix was incubated at 37°C for 2 min at 300 rpm. Untreated samples served as control. Crosslinking reactions were stopped by addition of Tris/HCl to a final concentration of 200 mM and incubated for 15 min at room temperature. Proteins were subjected to SDS-PAGE on Tris/acetate gels followed by silver staining as described below.

5.6.3 - Protease activity assays

Protease activity against BSA. 20 µl culture medium from HEK-293T cells overexpressing HTRA1 or from control non-transfected cells were added with 5 µg BSA (BioRad) and 1.5 mM DTT (Dithiothreitol). Samples were incubated at 37°C for up to 72 h and BSA degradation was evaluated by SDS-PAGE and Coomassie staining as described below.

Protease activity against physiological substrates. 20 µl culture medium from HEK-293T cells overexpressing HTRA1 or from control non-transfected cells were added with 5 µl of culture medium from cells overexpressing LTBP1, or 200 nM fibronectin (Sigma Aldrich) prepared in culture medium from control cells, in a Low Bind Eppendorf tube. Incubation at

37°C lasted for 1 h, 5 h or 24 h. Substrate cleavage was analysis by SDS-PAGE and immunoblot as described below.

5.6.4 - Polyacrylamide gel electrophoresis

5.6.4.1 - SDS-polyacrylamide gel electrophoresis

Protein samples (20-30 µl culture medium, 5-25 µg lysate, 0.5-2 µg purified HTRA1 or BSA) were denatured by addition of Laemmli buffer and incubation for 5 min at 95°C. For the comparative analysis of the intracellular, secreted and ECM fractions, 5 % of the total material retrieved from each fraction were analysed. 5 µl of Precision Plus Protein All Blue Standard (BioRad, 10,000-250,000 kDa) were included in each run.

The composition of the running and stacking acrylamide gels is shown in **Table 5**. Polymerisation was induced by addition of tetramethylethylenediamine (Temed, Carl Roth) and ammonium persulfate (APS) and gels were cast in a Mini-Protein casting device (1 mm gel thickness, 15-well combs, Bio-Rad). Electrophoresis was conducted for 1 h at 150 V in a Mini-Protean 3 device (Bio-Rad) filled with electrophoresis buffer (**Table 3**).

	H₂O distilled (ml)	Polyacrylamide solution 30 % (w/v) (ml)	Tris-base Solution (ml)	APS Solution 10 % (w/v) (µl)	Temed (µl)
Upper Gel (pH 6.8)					
	2.9	0.6	1.0	45	4.5
Lower Gel (pH 8.8)					
10 %	4.9	4.0	3.0	100	10
12 %	4.1	4.8	3.0	100	10
15 %	2.9	6.0	3.0	100	10

Table 5: Composition of the polyacrylamide gels.
Acrylamide/bis-acrylamide solution by National Diagnostics. APS: ammonium persulfate; Temed: tetramethylethylenediamine.

5.6.4.2 - Electrophoresis on Tris/Acetate gels

Following crosslinking, samples were added with DTT-free Laemmli buffer and were incubated at 40°C for 2 min. Electrophoresis was performed for 1 h 30 min to 2 h at 100 V using commercial NuPAGE Tris-Acetate gradient gels (3-8 %, Novex, Gibco Invitrogen), electrophoresis tanks from Gibco Invitrogen and a commercial NuPAGE Tris-Acetate SDS Running Buffer (Gibco Invitrogen). 0.25 µl HiMark™ Unstained Protein Standard (30,000-460,000 kDa, Gibco Invitrogen) were included in each run.

5.6.5 - Gel staining

Coomassie staining. Gels were covered with a colloidal Coomassie staining solution (**Table 3**) and gently agitated for 24 h at room temperature. After one rinse with dH_2O gels were scanned with an EPSON 1640SU using the software IrfanView (Irfan Skiljan).

Silver staining. Staining was performed with the Roti-Black P silver staining kit (Carl Roth). After fixation in a 3:1 volume methanol/acetic acid solution added with paraformaldehyde (PFA), and washings in 20 % (v/v) methanol, gels were sensitized for 1 min, washed with dH_2O and impregnated for 40 min at room temperature. Gels were gently agitated in the developing solution until protein bands were visible. The reaction was stopped in a 15 % (v/v) methanol, 9 % (v/v) acetic acid solution. Gels were rinsed with dH_2O and scanned as described above.

5.6.6 - Immunoblotting

Protein Transfer onto membranes. 0.45 μm polyvinylidene fluoride (PVDF) membranes (Immobilon-P; Millipore) were dipped in MetOH. Proteins were blotted on PVDF in a Mini-PROTEAN Tetra Cell and Blotting Module (BioRad) containing blotting buffer (**Table 3**) at 100 V for 45-60 min.

Immunodetection. Membranes were incubated in TBS-T (tris-buffered saline with Tween20) 4 % (w/v) skim milk for at least 15 min to minimize non-specific antibody binding, then with the primary antibody prepared in TBS-T/milk (**Table 6**) for 1-2 h at room temperature or overnight at 4°C. After 3 washings of 10 min with TBS-T, membranes were probed with the secondary, horseradish peroxidase-coupled (HRP) antibody diluted in TBS-T/milk (**Table 6**) for 1-2 h at room temperature. Following addition of Immobilon Western Chemiluminescent HRP Substrate (Millipore, 1ml of a 1:1 mix per membrane), a Fusion FX7 cooled camera (Fusion, Vilber Lourmat) was used to detect luminescence. Images were acquired with the Fusion software (Vilber Lourmat) and the ImageJ software (Fiji) was used for signal quantification.

Antigen	Host	Working dilution for immunoblots	Molecular mass (kDa)	Company
Primary antibodies				
Fibronectin	rabbit	1 : 5,000	262	Sigma-Aldrich
HTRA1	rabbit	1 : 1,000	51	S. Fauser (Univ. Cologne) [106]
Myc-tag	mouse	1 : 5,000	NA	Santa Cruz Biotechnology
Tubulin	mouse	1 : 1,000	50	Sigma-Aldrich
V5-tag	mouse	1 : 5,000	NA	Gibco-Invitrogen
Secondary antibodies (all HRP-coupled)				
Mouse Ig	goat	1 : 10,000	NA	Dako
Rabbit Ig	goat	1 : 10,000	NA	Dako

Table 6: Primary and secondary antibodies.
Antibodies are listed by alphabetic order. HRP: horseradish peroxidase-coupled; kDa: kilo Dalton.

5.6.7 - Solid phase binding assays

Maxisorp 96-well plates (Nunc) were coated overnight at 4°C with 20 µg/ml fibronectin (Sigma Aldrich), type I collagen (BD Bioscience), type IV collagen (Sigma Aldrich), or vitronectin (BD Bioscience) prepared in PBS (50 µl / well). After 3 washings with PBS and blocking with 1 % (v/v) BSA in PBS for 1 h at room temperature, culture medium from HEK-293T cells transfected to overexpress HTRA1 or from control non-transfected cells was added to the wells and incubated for 45 min at room temperature (100 µl / well). After washings, HTRA1 binding was detected by incubation with an anti-V5 tag antibody diluted 1:500 in PBS/0.1 % BSA for 45 min at room temperature, washings, and incubation with HRP-coupled anti-mouse IgG antibodies diluted 1:100 in PBS/BSA for 45 min at room temperature. Immune complexes were revealed by incubation with 100 µl of the HRP substrate tetramethylbenzidine (TMB) and the reaction was stopped by addition of 100 µl of an acidic stop solution (both Seracare Life Sciences Inc.). The optical density was measured at 560 nm, with a filter at 420 nm. After washings, bound proteins were solubilized in Laemmli buffer for 10 min at 80°C and HTRA1 was detected by immunoblot as described above.

5.7 - Statistical analysis and data representation

Statistical analysis was performed using the two-sided unpaired Student´s t-test or the Fisher´s exact test (biostatgv.sentiweb.fr). A p-value ≤ 0.05 was considered as significant. Excel (Microsoft), GraphPad Prism 6 (GraphPad Software Inc) and Power Point (Microsoft) were used to prepare the illustrations.

6 - Results

6.1 - Literature-based and *in silico* analysis of mutations within HTRA1 Mac-domain

The first 3 missense mutations within the HTRA1 Mac-domain (S121R, A123S and R133G) have been reported in the princeps cohort study which linked monoallelic *HTRA1* mutations to late onset familial SVD [27]. In the course of my experimental work, 3 additional pathogenic missense Mac-domain mutations have been reported (G120D, S136G and Q151K).

6.1.1 - Patient characteristics

Each of the 6 missense Mac-domain mutation has been identified in a single heterozygous patient, except Q151K, which has been detected in 2 unrelated cases. All cases met the criteria of CSVD neuroimaging findings (**Table 7**) and had a family history of stroke or dementia (**Supplementary Figure 1**).

Mac-domain mutation	G120D	S121R	A123S	A133G	S136G	Q151K	
Patient							
Gender	F	M	M	F	F	M	F
Risk factor	AHT	-	AHT	-	-	-	20 py
Age at onset	52	56	NA	NA	63	59	48
Age at diagnosis	53	66	50	58	77	60	52
Initial symptom	ICH	Balance impairment	Seizures	Headache	Gait disturbance	Gait disturbance	Seizures
Neuroimaging							
WMH	+	+	+	+	+	+	+
Lacunes	+	+	+	-	NA	-	NA
Microbleeds	NA	-	-	NA	NA	+	NA
Age at MRI	53	62	50	58	NA	60	48
Manifestations							
Stroke	+	-	-	-	+	-	-
Cognitive impairment	+	+	-	-	+	+	-
Dementia	-	+	-	-	-	-	-
Gait disturbance	-	+	-	-	+	+	-
Extraneurological manifestation	-	-	-	-	-	-	-
Reference	[64]	[27]	[27]	[27]	[63]	[63, 107]	ISD

Table 7: Characteristics of Mac-domain mutation carriers.
AHT: arterial hypertension; F: female; ICH: intracerebral hemorrhage; M: male; NA: not available; py: pack years (of smoking). The woman with mutation Q151K was detected in-house (ISD, unpublished observations); +: feature present; -: feature not present.

Gender and vascular risk factors. 4 out of 7 Mac-domain mutation carriers are females. Conversely, as shown in **Table 8**, symptomatic individuals carrying a heterozygous archetypal HTRA1 mutation (*i.e.*, a nonsense or a frameshift mutation before the catalytic serine (S328), or a missense mutation within the protease domain) consist of > 75 % males ($p = 0.08$; individual characteristics of patients carrying an archetypal HTRA1 mutation are provided in **Supplementary Table 1**). Similar to archetypical HTRA1 mutation carriers, about a third of the Mac-domain mutations carriers are hypertensive.

Disease onset and progression. The mean age at disease onset, which ranges between 48 and 63 years, is 55.6 years, slightly but not significantly lower than that reported for cases carrying an archetypical HTRA1 mutation (*i.e.*, mean 63.8 years). The earliest symptom is variable, ranging from headaches to stroke. Three out of 7 patients initially manifested with gait disturbance or balance impairment. In patients carrying an archetypal HTRA1 mutation, the first symptom is usually transient ischemic attack, ischemic stroke or cerebral hemorrhage, cognitive impairment, or gait disturbance/balance impairment (**Supplementary Table 1**). The mean age at diagnosis of Mac-domain mutation carriers is 59.4 years, while age at death has not been reported.

Neurological symptoms and MRI hallmarks. Out of 7 cases, 2 presented with ischemic stroke along with severe neurological manifestations (*i.e.*, cognitive impairment, dementia, and gait disturbance), 3 suffered severe neurological symptoms in the absence of stroke, while the remaining two were afflicted by milder symptoms. Notably, the prevalence of stroke and extraneurological symptoms is significantly higher in archetypal HTRA1 mutation carriers (each $p < 0.05$) while that of cognitive impairment, dementia or gait disturbance is comparable (**Table 8**). All symptomatic cases exhibit WMH. The other MRI features are not consistently reported in the literature, precluding reliable comparison. Lacunes tend to appear more frequently in archetypical HTRA1 mutation carriers, but this did not reach statistical significance ($p = 0.08$). An important limitation at this point is that no correction was made for covariate factors due to the small sample size.

Feature	Missense Mac-domain mutation carriers	Symptomatic archetypal mutation carriers	*p*-value
General			
Number of mutations detected	6	29	
Number of affected mutation carriers	7	56	
Gender	4 F, 3 M	13 F, 43 M	0.08
Arterial Hypertension (n; ratio)	2 (7; 29 %)	22 (50; 44 %)	0.69
Age of onset (mean ± SD in years) (n)	55.6 ± 5.9 (5)	63.8 ± 8.4 (54)	
Age of diagnosis (mean ± SD in years) (n)	59.4 ± 9.5 (7)	65.8 ± 7.0 (54)	
Manifestations			
Stroke (n; ratio)	2 (7; 29 %)	40 (54; 74 %)	**0.03**
Cognitive impairment (n; ratio)	4 (7; 57 %)	42 (51; 82 %)	0.15
Dementia (n; ratio)	1 (7; 14 %)	5 (50; 10 %)	0.56
Gait disturbance (n; ratio)	3 (7; 43 %)	31 (51; 61 %)	0.43
Extraneurological symptoms (n; ratio)	0 (7; 0 %)	25 (39; 64 %)	**<0.01**
Neuroimaging			
WMH (n; ratio)	7 (7; 100%)	52 (52; 100 %)	
Lacunes (n; ratio)	3 (5; 60 %)	38 (41; 93 %)	0.08
Microbleeds (n; ratio)	1 (3; 33 %)	18 (30; 60 %)	0.56
Age of neuroimaging (mean ± SD in years) (n)	55.2 ± 5.7 (6)	66.0 ± 2.8 (27)	

Table 8: Demographic and clinical characteristics of monoallelic Mac-domain and archetypal HTRA1 mutation carriers.
Archetypal HTRA1 mutations include nonsense and frameshift mutations resulting in the loss of one or more catalytic residues as well as missense mutations targeting the protease domain. Extraneurological symptoms include alopecia and spondylosis. Asymptomatic mutation carriers were excluded. Neuroimaging features are inconsistently reported, affecting reliable comparison. *p*-values were calculated by Fisher's exact test, excluding patients with unavailable data. F: female; M: male; SD: standard deviation; WMH: white matter hyperintensities.

6.1.2 - Mutation characteristics

Prevalence and predicted pathogenicity. Mutations G120D, S121R, A123S, R133G, S136G and Q151K are very rare (prevalence < 0.05 %) or are not detected in reference cohorts (**Table 9**). Moreover, they are estimated to be pathogenic by several independent *in silico* prediction tools (**Table 10**).

Missense mutations Mac-domain mutations		Frequency databases				
cDNA	amino acid change	1000 Genomes frequency	dbSNP (ALFA Allele Frequency)	ExAc	gnomAD	TOPMed
c.152 A>G	p.E51G*	absent	rs2097481474 (0.00009)	absent	absent	0.00227
c.176 G>C	p.R59P*	rs1246114252	rs1246114252 (0.00007)	absent	0.0001556	0.0295
c.359 G>A	p.G120D	rs1554948318	rs1554948318 (0.00000)	absent	absent	absent
c.361 A>C	p.S121R	absent	absent	absent	absent	absent
c.367 G>T	p.A123S	absent	absent	absent	absent	absent
c.397 C>G	p.R133G	absent	absent	absent	absent	absent
c.406 A>G	p.S136G	absent	absent	absent	absent	absent
c.446 T>C	p.V149A*	rs748995373	rs748995373 (0.00000)	absent	0.00001314	0.000378
c.451 C>A	p.Q151K	rs754645487	rs754645487 (0.00017)	0.0001868	0.0001905	0.0174

Table 9: Frequency of missense mutations within the HTRA1 Mac-domain.
*: R59P, E51G and V149A are considered as non-pathogenic (see Table 10). References of the databases are reported in Section 5.2.

Of note, some familial CSVD cases carrying R59P, E51G and V149A have been identified. R59P and V149A appear in other databases, although with a rather low frequency (< 1%). More importantly, all three mutations are classified as benign by independent *in silico* prediction tools. Therefore, they were considered as non-pathogenic and not further evaluated.

Missense mutations within HTRA1 Mac-domain		*In silico* databases				
cDNA	amino acid change	PolyPhen2 (HumVar)	SIFT	Mutation Taster	Provean	Mutations Assessor*
c.152 A>G	p.E51G	Benign	Tolerated	Polymorphism	Neutral	Neutral
c.176 G>C	p.R59P	Benign	Tolerated	Polymorphism	Neutral	Neutral
c.359 G>A	p.G120D	Probably damaging	Affect protein function	Disease causing	Deleterious	High
c.361 A>C	p.S121R	Possibly damaging	Deleterious	Disease causing	Deleterious	High
c.367 G>T	p.A123S	Possibly damaging	Tolerated	Disease causing	Neutral	Neutral
c.397 C>G	p.R133G	Possibly damaging	Tolerated	Disease causing	Deleterious	Low
c.406 A>G	p.S136G	Benign	Damaging	Disease causing	Neutral	Medium
c.446 T>C	p.V149A	Benign	Tolerated	Polymorphism	Neutral	Low
c.451 C>A	p.Q151K	Possibly damaging	Affect protein function	Disease causing	Deleterious	Low

Table 10: *In silico* prediction of HTRA1 Mac-domain mutations pathogenicity.
*: The *Mutations Assessor* predicts the functional impact of missense mutations in proteins. References of the *in silico* tools are reported in Section 5.2.

Position of the residues targeted by pathogenic mutations. Interestingly, all pathogenic missense mutations within the Mac-domain are restricted to the Kazal-domain (**Figure 6**). When normalized to the length of the respective HTRA1 domains, unique missense mutations within this domain are significantly more frequent than IGFBP- or PDZ-domain mutations (*i.e.*, > 13.5 mutations / 100 aa vs 0 and < 2 mutations / 100 aa; $p < 0.005$). In fact, they even appear as frequent as missense mutations within the protease-domain (*i.e.*, > 15 mutations / 100 aa; $p = 1$). As describe in the Introduction, the function of the Kazal-domain is unknown. It is structurally defined by an arrangement of disulfide bonds. Of note, mutations reported so-far leave the corresponding cysteine residues unaffected.

Together, two new and important aspects are highlighted: First, Mac-domain mutations carriers exhibit classical CSVD features, but their phenotype appears milder than that of cases carrying archetypal HTRA1 mutations. Second, disease-related Mac-domain mutations are restricted to the Kazal-domain.

6.2 - Intracellular stability of Mac-domain mutant HTRA1

6.2.1 - Protein expression and secretion

As an initial step to evaluate the functional consequences of missense Mac-domain mutations, human HEK-293T cells were transfected to overexpress HTRA1. Non-transfected cells (-), as well as cells overexpressing HTRA1 WT or an inactive mutant (S328A), obtained by replacement of the catalytic serine by an alanine, served as positive and negative controls, respectively. Culture medium was collected, and cells were lysed, followed by detection of recombinant HTRA1 in the intracellular and extracellular fractions by anti-Myc immunoblot. **Figure 7A** shows representative images and **Figure 7B** depicts the quantitative analysis of the behavior of HTRA1 WT, S328A, R133G and Q151K.
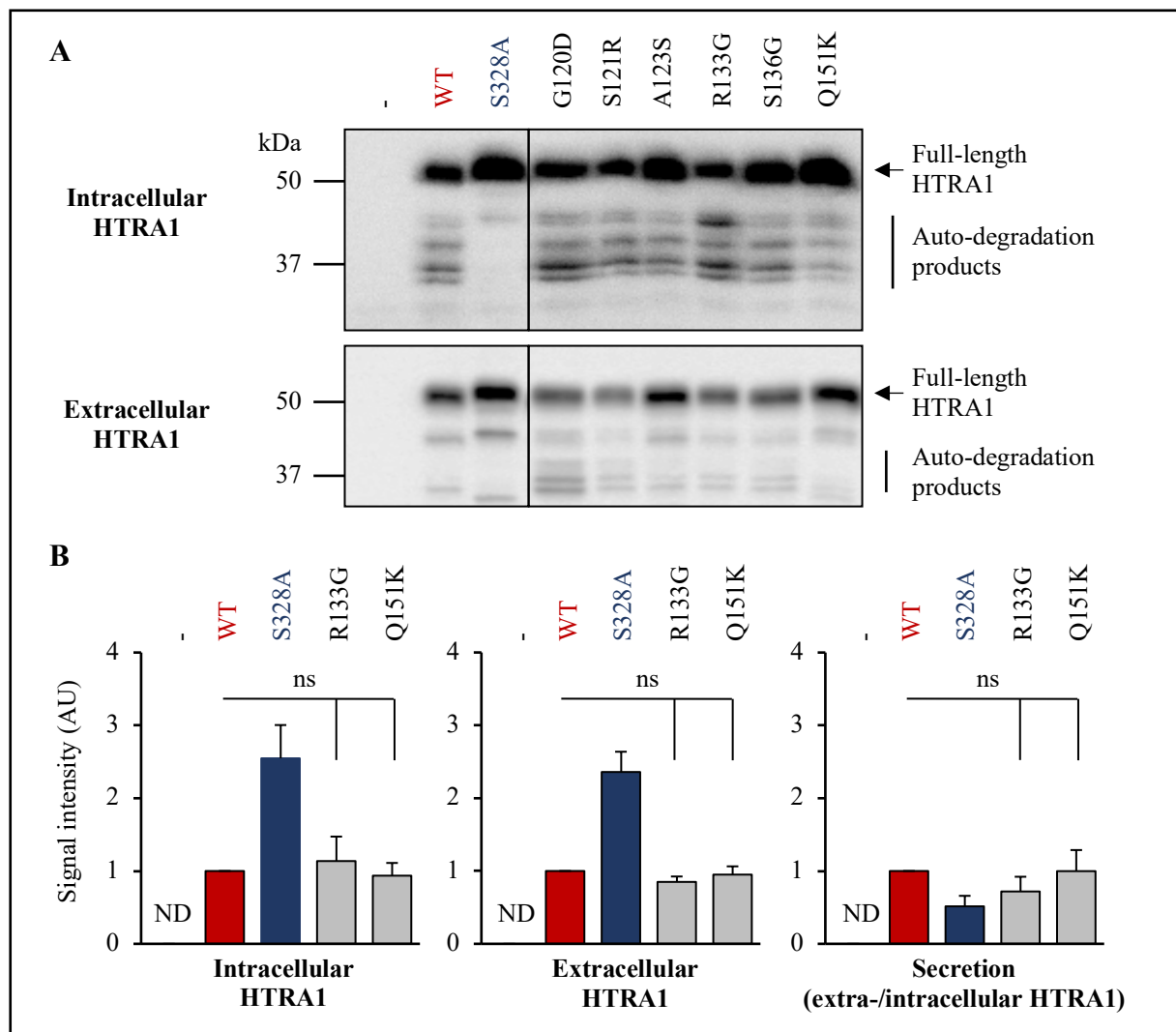
Figure 7: Expression and secretion of recombinant Mac-domain mutant HTRA1.
A: Following overexpression, intra- and extracellular recombinant HTRA1 was detected by immunoblot in the cell lysates and culture media, respectively. B: Histograms depict the mean + standard error of the mean (SEM) signal intensity measured in 3 independent experiments. The signal of HTRA1 WT was set to 1, *p*-value was calculated by Student´s *t*-test. AU: arbitrary units; ND: not detected; ns: non-significant; -: control, non-transfected cells.

All six Mac-domain mutants are detected in the cell lysate (*i.e.*, the intracellular fraction) and in cell culture medium (*i.e.*, the extracellular fraction) (**Figure 7A**). Mutants R133G and Q151K were randomly selected for detailed analysis: protein abundancy in the intra- and extracellular fractions, as well as the extra-/intracellular ratios are similar to those measured for HTRA1 WT, indicating that R133G and Q151K are normally expressed and secreted (**Figure 7B**).

Of note, lower molecular mass HTRA1 species (*i.e.*, around 37 kDa compared to the 51 kDa FL HTRA1), resulting from the proteolytic auto-degradation of HTRA1 [73] are detected in intra- and extracellular extracts from cells overexpressing HTRA1 WT or Mac-domain mutant (the protease activity of the mutants is reported in section 6.4) [94]. The inactive variant S328A, which does not auto-lyse, exhibits a distinct, less fragmented pattern. Along with this, HTRA1 WT and Mac-domain mutants are less abundant than S328A both intra- and extracellularly.

6.2.2 - Protein steady-state levels and stability

Further, the stability of the Mac-domain mutants in overexpressing HEK-293T cells was evaluated focusing on mutants S121R, A123S and R133G. HTRA1 degradation by auto-proteolysis is exacerbated by overexpression and might thus not reflect a physiological process. Therefore, the expression and stability of these mutants was investigated both in a WT and in an inactive (S328A) background.

Steady-state protein abundancy. Analysis of the protein steady-state levels indicated that as described in the previous paragraph, S121R, A123S and R133G abundancy is comparable to the abundancy of HTRA1 WT both intra and extracellularly (**Figure 8**). Inactivation of A123S and R133G by addition of a S328A mutation impairs their auto-degradation, as judged by the disappearance of the auto-degradation fragments (see intracellular extracts) and results in their intra- and extracellular accumulation, exactly as seen for the conversion of WT into S328A. S121R-S328A behaves as the two other inactive Mac-domain mutants within the cells (*i.e.*, reduced degradation products and accumulation), however it is markedly less abundant extracellularly.
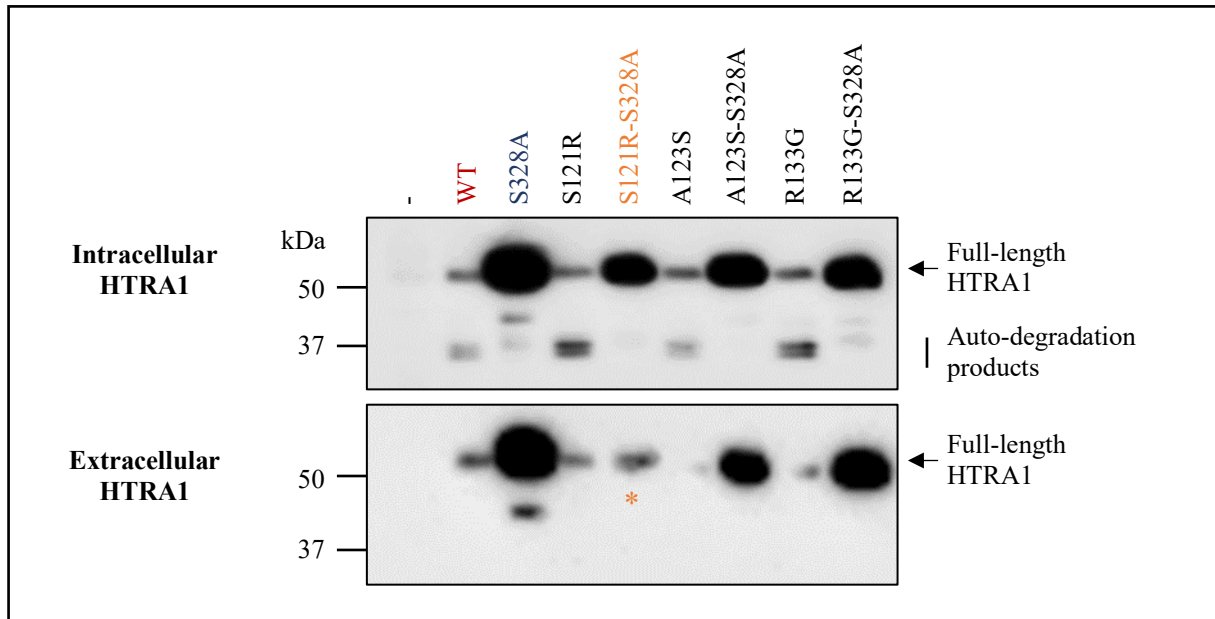
Figure 8: Expression and secretion of proteolytically inactive Mac-domain mutant HTRA1.
The activity of the Mac-domain mutant proteins was abrogated by the addition of an active site mutation (S328A). Following overexpression, intra- and extracellular recombinant HTRA1 was detected by immunoblot in the cell lysates and culture media, respectively. Results are representative of 2 independent experiments. *Low extracellular S121R-S328A levels. -: control, non-transfected cells.

Intracellular protein stability. To follow up, the intracellular stability of the above-mentioned active and inactive HTRA1 mutants was evaluated. Therefore, HTRA1-overexpressing HEK-293T cells were treated with the cell-permeable protein translation inhibitor cycloheximide for increasing time periods and the disappearance of HTRA1 in the cell lysates was monitored by immunoblot (**Figure 9A and B**). Cycloheximide-free samples (-) served as controls. Similar to HTRA1 WT, S121R, A123S and R133G are rapidly degraded (*i.e.*, $t_{1/2} < 1.5$ h; $t_{1/2}$ is the treatment time resulting in the disappearance of 50 % of HTRA1; > 80 % degradation is achieved within 5 h). Conversely, > 30 % S328A, A123S-S328A and R133G-S328A are detected up to 5 h exposure to cycloheximide ($t_{1/2} > 1.5$ h). S121R-S328A, exhibits a distinct pattern, as it is rapidly degraded ($t_{1/2} < 0.5$ h; > 90 % degradation is achieved within 5 h), similar to the active HTRA1 variants, including HTRA1 WT and S121R.
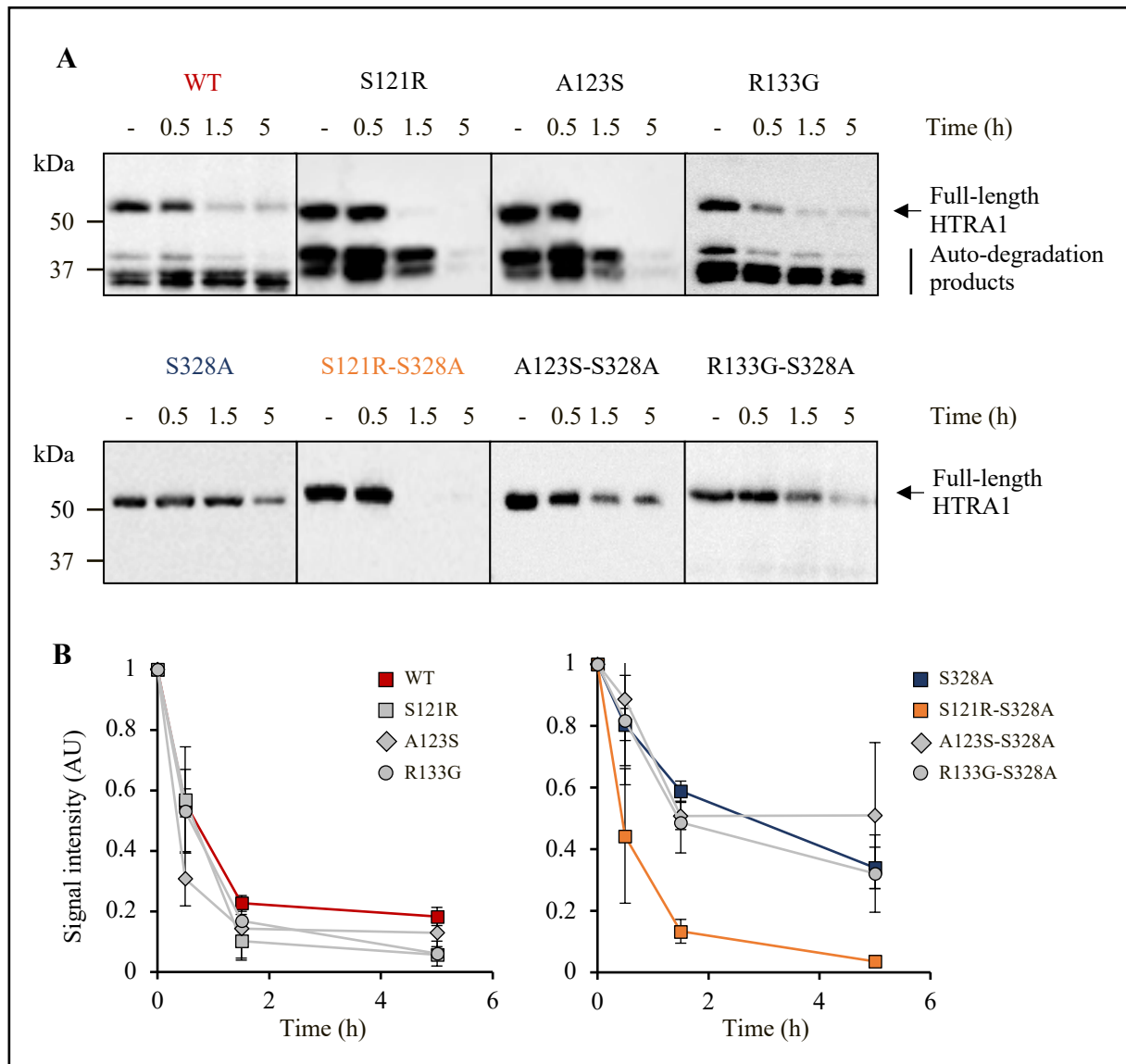
Figure 9: Intracellular stability of Mac-domain mutant HTRA1.
A: HEK-293T cells were transfected to overexpress HTRA1, then treated with cycloheximide for 0.5, 1.5 or 5 h and lysed. Cycloheximide-free cells (-) were prepared as control. HTRA1 abundancy was evaluated by immunoblot. B: Graphs depict the mean + SEM signal intensity measured in 3-4 independent experiments. HTRA1 signal in cycloheximide-free cells was set to 1. AU: arbitrary units.

In conclusion, following overexpression in human cells, Mac-domain mutants exhibit a normal intracellular behavior and secretion with exception of mutant S121R which displays a markedly reduced intracellular stability along with reduced abundancy in the extracellular space.

6.3 - Conformation of Mac-domain mutant HTRA1

To complement cell-based assays, the conformation of purified proteins was examined.

6.3.1 - Protein purification

Auto-degradation of HTRA1 impairs the purification of the protein in its active form. Therefore, the pathogenic HTRA1 mutants were all purified as inactive proteins and the active site mutant S328A served as control. HTRA1 was purified from the secretome of HEK-293T cultures stably transfected to overexpress HTRA1 and serum starved. Protein purification was performed taking advantage of the carboxyterminal His6-tag, according to the following steps: (i) dialysis against PBS, (ii) binding to a Co^{2+}-resin, (iii) washes, (iv) EDTA-based elution, (v) final dialysis against Tris/NaCl or PBS. Aliquots were collected at each step and the protein content was evaluated by SDS-PAGE and Commassie staining (**Figure 10A**). The procedure results in protein preparations which display HTRA1 concentrations in the range 0.1-1 mg/ml and exhibit only minor contaminants (**Figure 10B**).
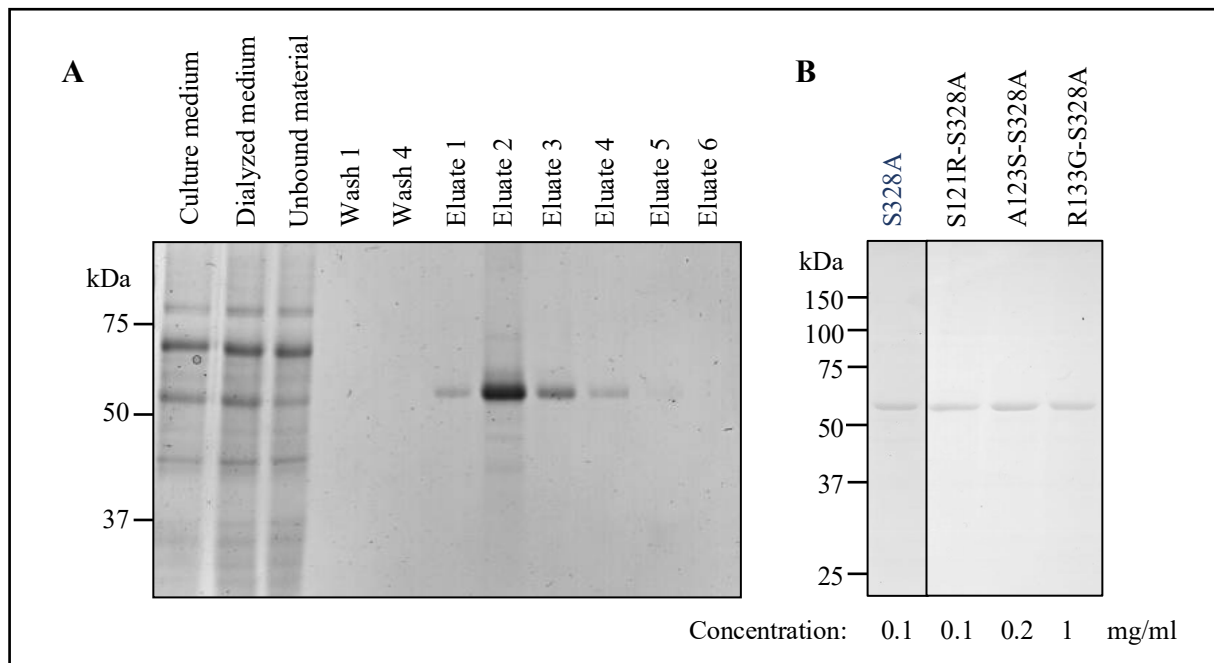
Figure 10: His6-tag based purification of Mac-domain mutant HTRA1.
A: Culture medium from cells overexpressing HTRA1-S328A was dialyzed and incubated with a His6-tag binding resin, followed by washing and elution. An aliquot of the relevant fractions was analyzed by SDS-PAGE and Coomassie staining. B: 1 μg of purified HTRA1 was analyzed by SDS-PAGE and Coomassie staining. HTRA1 protein concentrations in the stock solutions are provided at the bottom of the gel.

6.3.2 - Resistance to limited trypsin-digestion

Protein conformational changes can expose or mask putative protease cleavage sites. As an initial indicator of HTRA1 tertiary and/or quaternary conformation, I thus performed limited trypsin digestion assays [108]. Specifically, I exposed HTRA1 to trypsin for increasing time periods and examined the kinetic and pattern of HTRA1 degradation by SDS-PAGE and Coomassie staining. A trypsin-free sample (-) served as control.

As shown in **Figure 11**, the time course of hydrolysis of S328A, A123S-S328A and R133G-S328A are comparable ($t_{1/2}$ < 1 min, complete degradation is achieved within 5 - 7.5 min), as are the 50 kDa and 30 kDa degradation products generated. The degradation of S121R-S328A is markedly slower ($t_{1/2}$ > 1 min, only 90 % degradation is achieved within 15 min) and produces a distinct 40 kDa fragment.
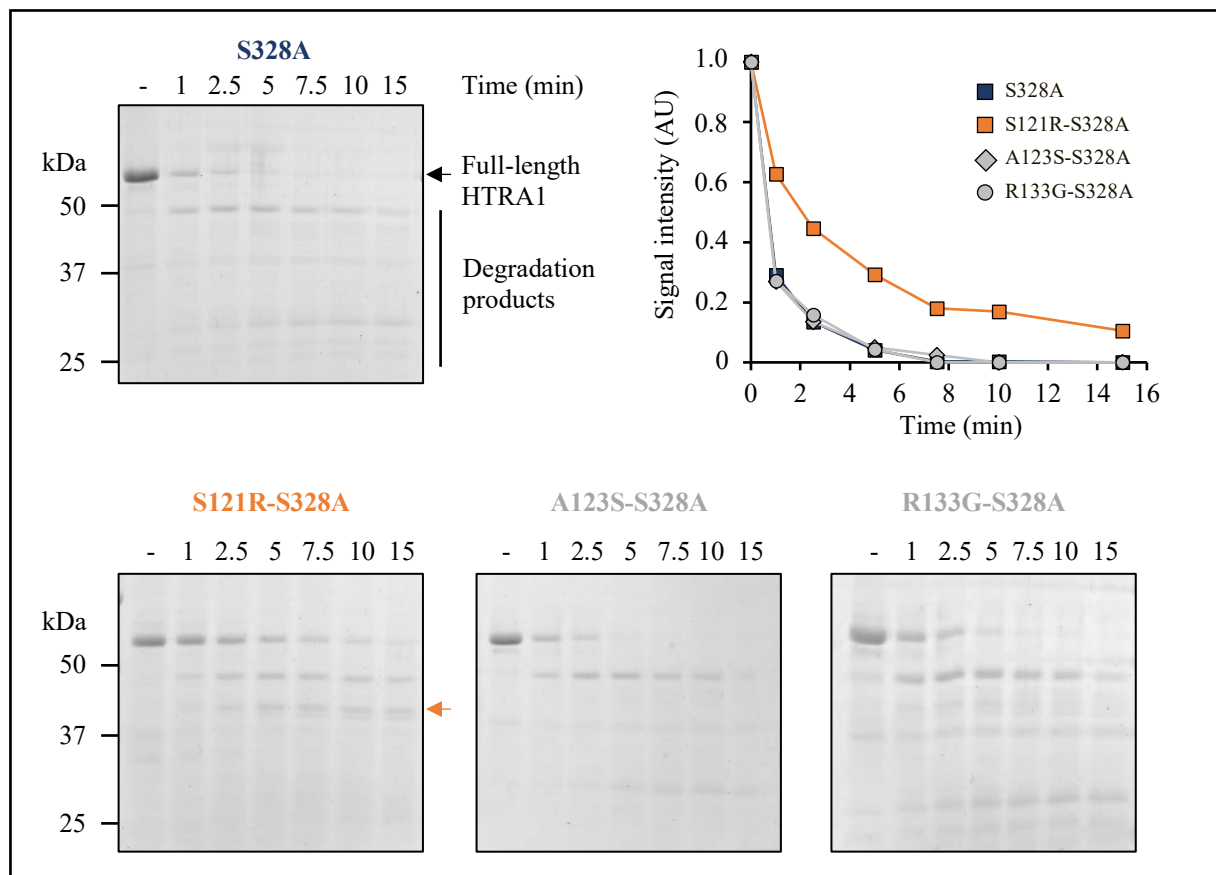
Figure 11: Resistance to limited trypsin digestion of Mac-domain mutant HTRA1.
Gels: Proteins were incubated with trypsin for the indicated time periods and analyzed by SDS-PAGE and Coomassie staining. Trypsin-free samples (-) were prepared as control. Orange arrowhead: S121R-S328A-specific degradation product. Graph: The disappearance of intact HTRA1 was quantified. Signal in trypsin-free samples was set to 1. AU: arbitrary units; blue: 2 independent batches of purified S328A.

6.3.3 - HTRA1 oligomeric state

As introduced, HTRA1 is in a dynamic equilibrium between monomers and homo-trimers [54]. Importantly, homo-trimerization is crucial for protease activity [82]. Therefore, the oligomeric state of the Mac-domain mutants was assessed. In this purpose, purified HTRA1 was subjected to the protein crosslinking agent glutaraldehyde (GA), which reacts with amine groups of lysine residues to generate thermally and chemically stable crosslinks, followed by SDS-PAGE and silver staining. S328A served as positive control and the pathogenic mutant G295R, a proteolytically inactive variant that fails trimerizing [94], as negative control. In addition, GA-free samples were prepared as controls (**Figure 12**).

In the absence of GA, all HTRA1 species migrate as 51 kDa monomers. As expected, crosslinked S328A is mostly present as > 150 kDa trimers whereas G295R exclusively forms monomers (and dimers) in the presence of GA. Similar to S328A, A123S-S328A and R133G-S328A form trimeric complexes, whereas S121R-S328A exists as a mix of monomeric, dimeric and trimeric species.
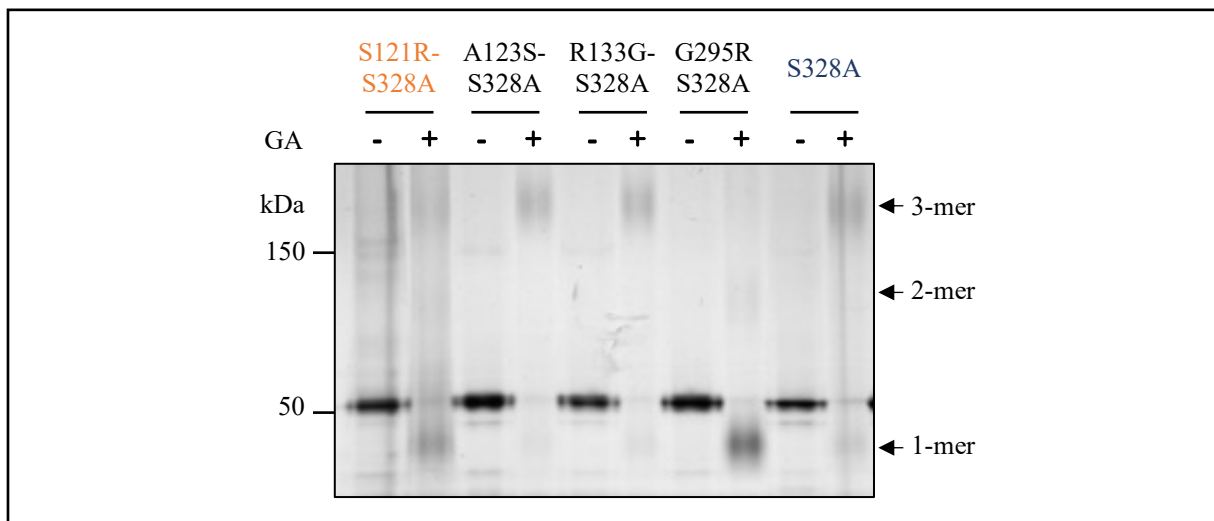
Figure 12: Oligomeric state of Mac-domain mutant HTRA1.
Purified HTRA1 was incubated with (+) or without (-) glutaraldehyde (GA) and analysed by SDS-PAGE and silver staining. The gel depicted is representative of 3 independent crosslinking assays. Monomers, dimers, and trimers are marked by arrowheads on the right-hand side. Note that GA increases the electrophoretic motility of HTRA1 monomers.

Together, these data indicate that mutation S121R alters the conformation of HTRA1. This mutation might result in partial misfolding of the corresponding mutant protein, providing a mechanistic basis for the reduced intracellular stability reported in the previous section. Conversely, the other tested Mac-domain mutants exhibit a normal molecular phenotype.

6.4 - Protease activity of Mac-domain mutant HTRA1

In parallel to the cell-based and biochemical assays described above, the protease activity of the Mac-domain mutants was studied using culture medium from HTRA1 overexpressing HEK-293T cells. Medium from non-transfected cells (-), and cells overexpressing HTRA1 WT served as controls.

6.4.1 - Enzymatic activity towards an analytical substrate

While native BSA is not degraded by HTRA1, it is efficiently cleaved under slightly denaturing conditions [109]. Therefore, I exposed BSA added with a low concentration of DTT to culture medium from HTRA1-overexpressing cells or of control cells for increasing time periods and evaluated BSA degradation by SDS-PAGE followed by Coomassie staining. HTRA1 abundancy within the samples was determined by immunoblot to confirm that they exhibit comparable amounts of protease (**Figure 13**, upper panel). As shown in **Figure 13**, lower panel, treatment of BSA with HTRA1 WT results in a progressive, time-dependent loss of intact BSA, along with the generation of multiple degradation products. Upon exposure to S121R, A123S or R133G, the kinetic and pattern of BSA degradation resembles that observed with HTRA1 WT, indicating that they exhibit a comparable protease activity.
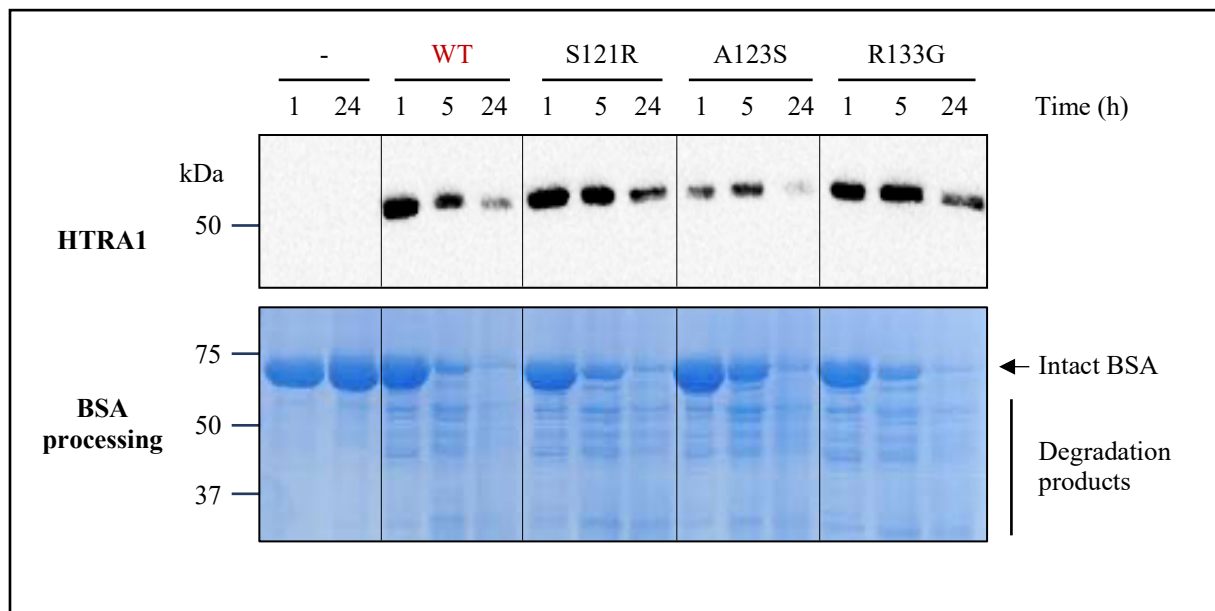
Figure 13: Protease activity of Mac-domain mutant HTRA1 towards the analytical substrate BSA.
BSA was exposed to culture medium from HTRA1-overexpressing cells or from non-transfected cells (-) for increasing time periods. HTRA1 abundancy was analysed by anti-Myc immunoblot (upper panel) and BSA degradation by SDS-PAGE and Coomassie staining (lower panel). Note the reduction of HTRA1 levels for long exposure times, reflecting auto-degradation. The data depicted are representative of 2 independent assays.

6.4.2 - Enzymatic activity towards physiological substrates

The analysis of HTRA1 protease activity was extended to physiological substrates. Specifically, fibronectin and LTBP1 were used, two targets of HTRA1 reported to accumulate in the brain vasculature of HTRA1-deficient mice [17]. Exposure of fibronectin or LTBP1 to HTRA1 WT results in their limited proteolysis, with conversion of the full proteins in a distinct cleaved product (**Figure 14A**). Of note, the processing of LTBP1 appears markedly more efficient than that of fibronectin, in accord with the fact that brain vessels from HTRA1-deficient mice exhibit a > 9-fold increase of LTBP1 abundancy compared to a < 2-fold increase of fibronectin abundancy [17]. As seen for BSA, the *in vitro* processing of fibronectin and LTBP1 by S121R, A123S or R133G is comparable to that observed upon treatment with HTRA1 WT (**Figure 14A**; HTRA1 detection by immunoblot within the culture media used for cleavage assay is depicted in **Figure 13**).
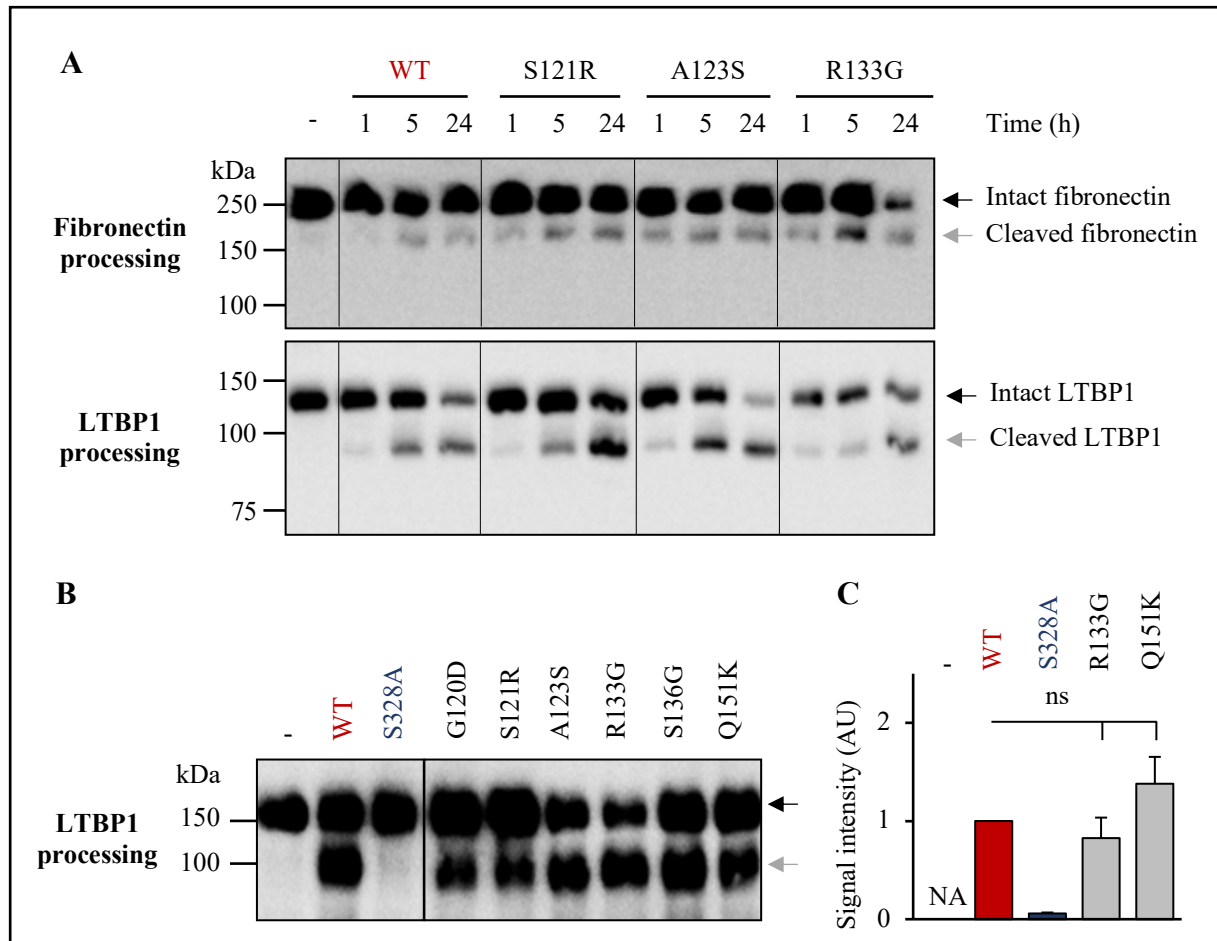
Figure 14: Protease activity of Mac-domain mutant HTRA1 towards physiological substrates.
A, B: Fibronectin (upper panel) or LTBP1 (lower panel) were exposed to culture medium from HTRA1-overexpressing cells or from control cells (-). Intact (black) and cleaved (grey) fibronectin and LTBP1 are marked by arrowheads. HTRA1 abundancy in culture medium was evaluated by immunoblot and is depicted in **Figure 13**, upper panel (for panel A) and in **Figure 7A**, lower panel (for panel B). C: HTRA1 protease activity was measured as the ratio cleaved/intact LTBP1 and was normalized to HTRA1 abundancy. Histograms depict the mean + SEM of 4 independent assays. The signal of HTRA1 WT was set to 1; p was calculated by Student´s t-test. AU: arbitrary units; NA: not applicable; ns: non-significant.

Using LTBP1 as substrate and experimental conditions resulting in incomplete proteolysis indicated that the protease activity of all 6 Mac-domain mutants is comparable to that of HTRA1 WT (**Figure 14B**; HTRA1 detection by immunoblot within the culture media used for cleavage assay is depicted in **Figure 7A**). Finally, for detailed analysis, focus was set on R133G and Q151K (**Figure 14C**): The ratio cleaved/intact LTBP1 was measured and normalized to HTRA1 abundancy in the culture medium, to account for marginal differences in HTRA1 levels. This semi-quantitative measurement further confirms that R133G and Q151K exhibit a protease activity similar to that of HTRA1 WT.

Collectively, these observations confirm that Mac-domain mutations do not impair the enzymatic activity of HTRA1 against the analytical substrate BSA in vitro *and extend this property to the physiological HTRA1 substrates fibronectin and LTBP1.*

6.5 - HTRA1 integration into the ECM

6.5.1 - Development of an experimental model to investigate the incorporation of recombinant HTRA1 in the ECM

HTRA1 is known to process various ECM and ECM-associated proteins (see Introduction). Moreover, my host laboratory reported that HTRA1 is present in the core matrisome of vascular tissues (*i.e.*, aorta, [85]). Consistently, compartment-resolved analysis of fibroblast cultures of HTRA1$^{+/+}$ mice (**Figure 15A**) indicates that endogenous HTRA1 distributes as follows: ca 10 % of total HTRA1 is present in the intracellular fraction (I) while ca 70 % is present in the secreted fraction (S). Most importantly, ca 20 % of total HTRA1 is detected in the ECM (M). These observations suggest that the interaction of HTRA1 with matrisomal proteins and its insertion in the ECM might be an important feature, which could locally increase HTRA1 concentration and catalyze the cleavage of the ECM and ECM-associated HTRA1 substrates.
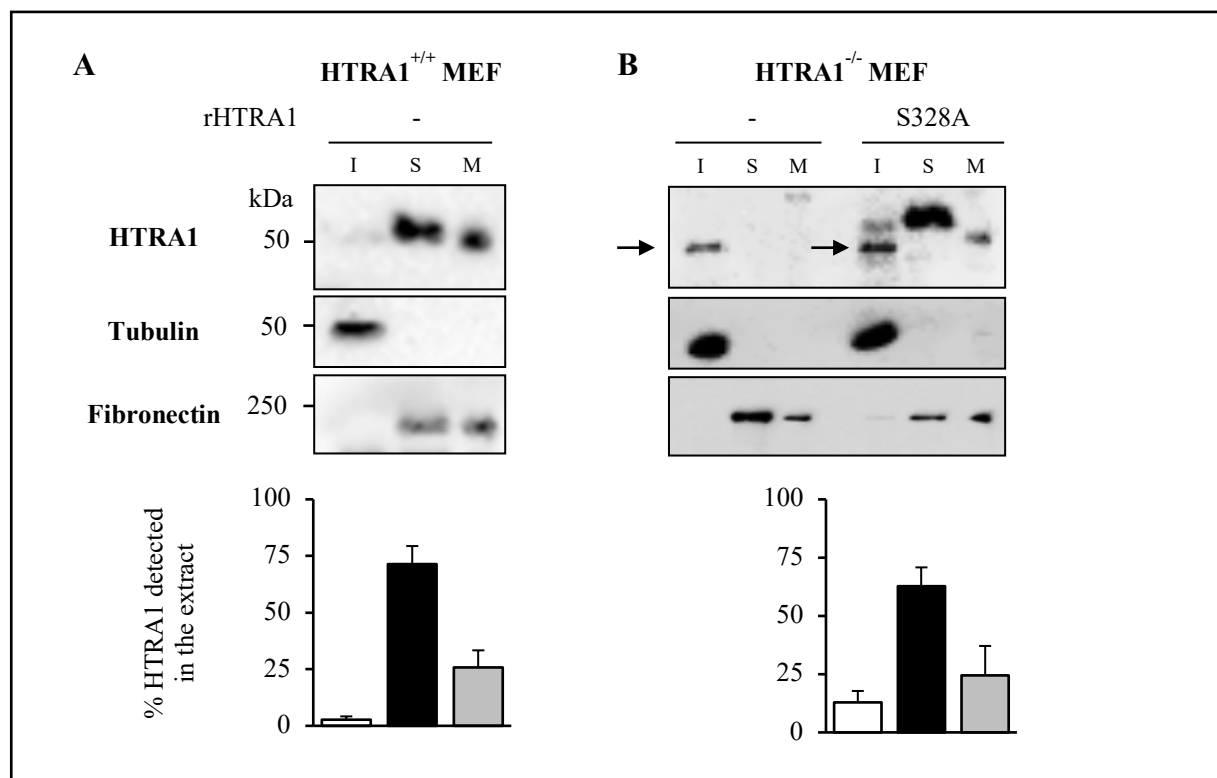
Figure 15: Distribution of endogenous and recombinant HTRA1 in mouse fibroblast subcellular fractions. A: Fibroblasts derived from HTRA1$^{+/+}$, or B: HTRA1$^{-/-}$ mouse embryos were left untreated (-) or transfected to overexpress recombinant HTRA1 (rHTRA1; S328A). The tubulin-rich intracellular (I) fraction, as well as the fibronectin-rich secreted (S) and ECM (M) fractions were collected and analysed by immunoblot using anti-HTRA1, anti-tubulin and anti-fibronectin antibodies (upper panels). Arrowheads point to an unspecific band detected in the lysates of control and transfected cells. Lower panels: HTRA1 signal intensity was quantified in each fraction and expressed as a percentage of total HTRA1.

To investigate the impact of Mac-domain mutations on the ECM insertion of HTRA1, an experimental model for the analysis of the subcellular distribution of recombinant HTRA1 was developed. For this, HTRA1$^{-/-}$ fibroblasts were used, transfected to overexpress inactive HTRA1, followed by collection and immunoblot analysis of the intracellular (I), secreted (S) and ECM (M) fractions. Non-transfected cells (-) served as control.

As shown in **Figure 15B**, recombinant, inactive HTRA1 (rHTRA1; S328A) distributes as follows: ca 25 and 55 % of total HTRA1 is present in the intracellular and secreted fraction, respectively, indicating an increased intracellular retention, compared to endogenous HTRA1. Similar to endogenous HTRA1, ca 20 % of total recombinant HTRA1 is detected in the ECM.

6.5.2 - Identification of the HTRA1 domain(s) involved in its insertion in the ECM

To uncover the HTRA1 domain(s) that mediate(s) its deposition in the ECM, the behavior of truncated recombinant proteins, lacking the Mac- (*i.e.*, ΔMac) or the PDZ-domain (*i.e.*, ΔPDZ) (**Figure 16A**), was analyzed. As shown in **Figure 16B**, the distribution of ΔPDZ-HTRA1 mimics that of FL-HTRA1. Conversely, the ΔMac-HTRA1 variant is significantly reduced in the ECM fraction, suggesting that the Mac-domain drives HTRA1 incorporation in the ECM. To complement these observations, the distribution of a HTRA1 variant exclusively composed of the Mac-domain (**Figure 16C**), was investigated. As seen in two representative examples, the presence of Mac-HTRA1 in the ECM is highly variable among assays, precluding conclusion.
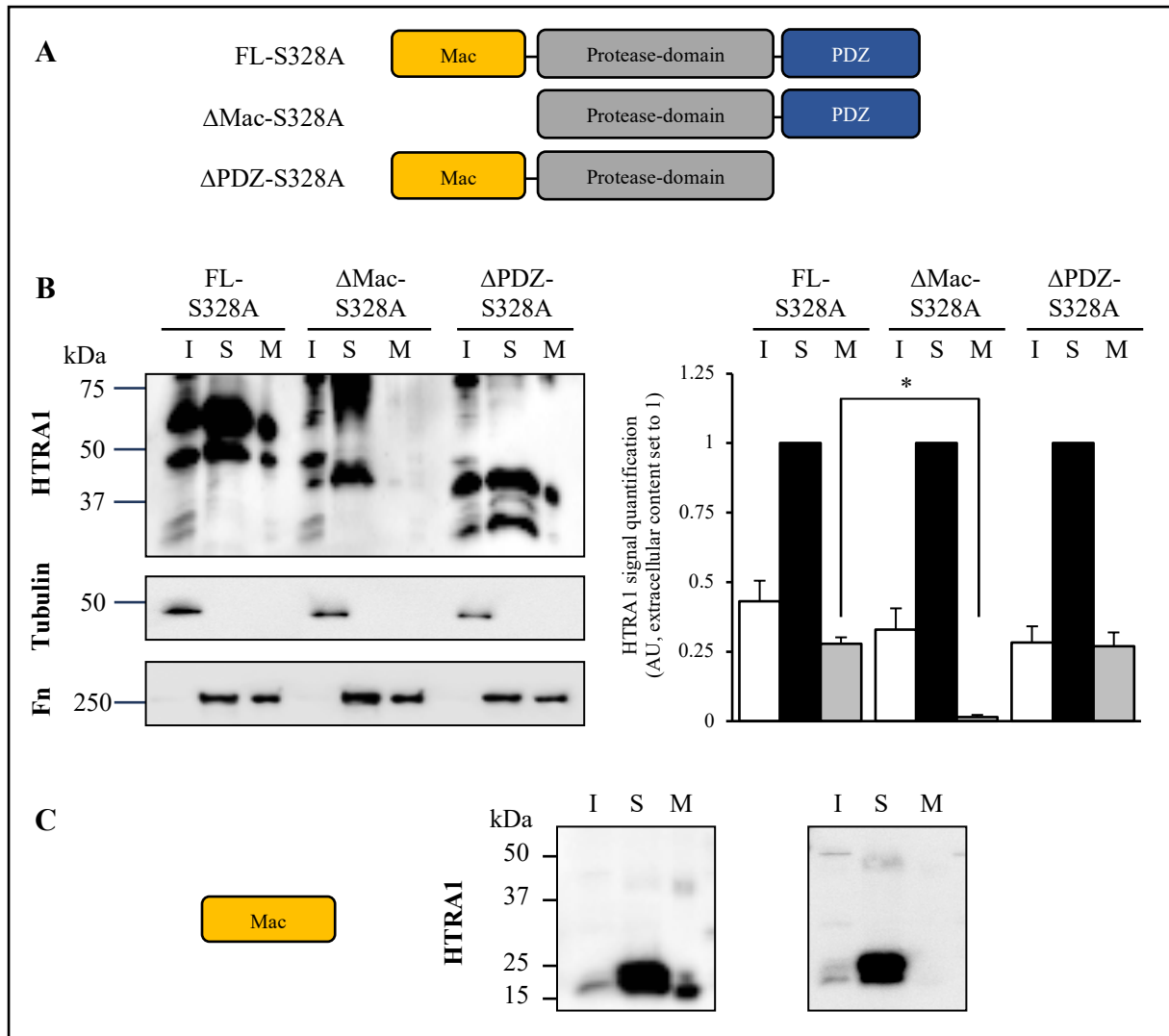
Figure 16: Distribution of truncated HTRA1 variants in mouse fibroblast subcellular fractions.
A: HTRA1$^{-/-}$ fibroblasts were transfected to overexpress full-length (FL) HTRA1, or truncated variants lacking the Mac- (ΔMac) or the PDZ-domain (ΔPDZ). B: The intracellular (I), secreted (S) and ECM (M) fractions were collected and analysed by immunoblot using anti-HTRA1(V5), anti-tubulin and/or anti-fibronectin (Fn) antibodies. Histograms depict the mean + SEM HTRA1 signal of 4 independent assays. Secreted HTRA1 signal was set to 1. C: The intracellular (I), secreted (S) and ECM (M) fractions of HTRA1$^{-/-}$ fibroblasts, transfected to overexpress the Mac-HTRA1 domain only, were collected and analysed by immunoblot using anti-HTRA1(V5). The ECM incorporation of the Mac-HTRA1 is variable among assays. AU: arbitrary units. p was calculated by t-test.

6.5.3 - Identification of the ECM partners of HTRA1

A solid phase binding assay was used to identify the ECM interactants of HTRA1 (**Figure 17A**). Specifically, purified vascular ECM proteins (vitronectin, fibronectin, type I or type IV collagen) were immobilized in a 96-well plate. Untreated (-) and/or poly-L-lysin (polyL) coated wells served as controls. After incubation with culture medium from HTRA1-overexpressing cells, Myc-tagged, bound HTRA1 was immunodetected using an ELISA-like procedure (**Figure 17B**). In complement, bound proteins were solubilized and HTRA1 was detected by anti-Myc immunoblot (**Figure 17C**).
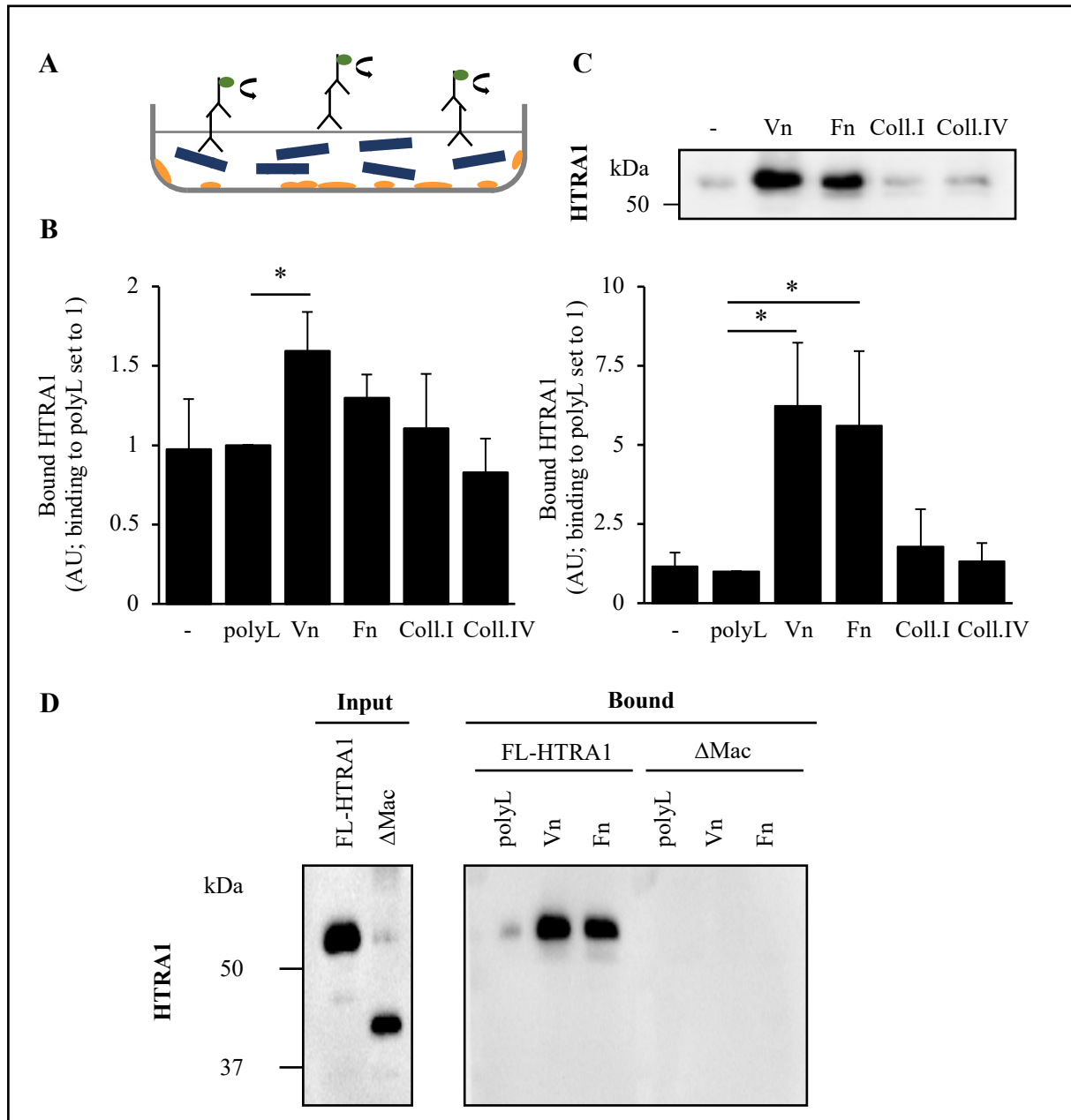
Figure 17: Binding of HTRA1 to purified matrix proteins.
A: Outline of the solid-phase binding assay. Purified ECM proteins (Vn: vitronectin, Fn; fibronectin, Coll.I: type I collagen, Coll. IV: type IV collagen) were immobilized on plastic. Alternatively, wells were left untreated (-) or coated with poly-L-lysin (polyL). Following incubation with culture medium of cells overexpressing HTRA1, bound HTRA1 was immunodetected using anti-V5 antibodies. Wells exposed to HTRA1-free culture medium were prepared to measure unspecific antibody binding (not illustrated). B: Histogram depicts the mean + SEM absorbance measured in 4 independent assays. C: Following absorbance measurement, proteins were solubilized and bound HTRA1 was detected by anti-V5 immunoblot. Histogram depicts the mean + SEM HTRA1 signal measured in 4 independent assays. The absorbance in poly-L-lysine coated wells was set to 1. D: The binding of full-length (FL) or ΔMac-HTRA1 (ΔMac) (input depicted on the left panel) to poly-L-lysine, vitronectin or fibronectin was assessed as in panel C. Images are representative of 2 independent assays. For B and C: The absorbance in poly-L-lysine coated wells was set to 1. AU: arbitrary units. p was calculated by t-test.

As shown in **Figure 17B and C**, a significant binding of HTRA1 to immobilized vitronectin (Vn) and fibronectin (Fn) was observed, compared to plastic and/or poly-L-lysin. Conversely, I found no interaction of HTRA1 with collagen I or IV. Together, this highlights vitronectin and fibronectin as putative ECM partners of HTRA1.

I further evaluated the binding of ΔMac-HTRA1 (ΔMac) to vitronectin and fibronectin (**Figure 17D**). In accord with the ECM insertion assays (**Figure 16B**), I found that the binding of ΔMac was markedly reduced compared to the binding of FL-HTRA1.

6.5.4 - ECM insertion of Mac-domain mutant HTRA1

Using HTRA1$^{-/-}$ fibroblasts transfected to overexpress recombinant HTRA1, the ECM insertion of the Mac-domain mutants S121R and A123S was assessed and compared to that of WT HTRA1, using FL (**Figure 18A**) or Mac-domain (**Figure 18B**) constructs. As depicted, the insertion of mutant HTRA1 was similar to that of WT HTRA1, speaking against an impact of the mutations on the incorporation of HTRA1 in the ECM.
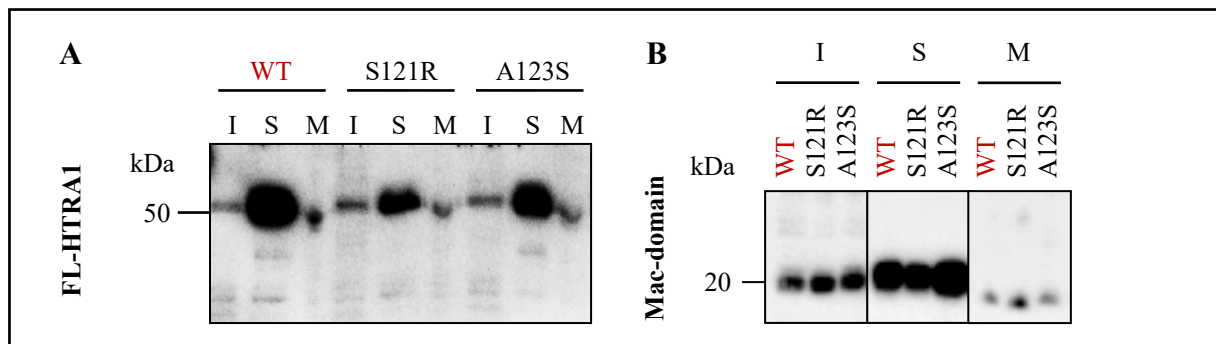
Figure 18: Insertion of Mac-domain mutant HTRA1 in the ECM of mouse fibroblasts.
A: HTRA1$^{-/-}$ fibroblasts were transfected to overexpress full-length HTRA1 (FL), or B: Mac-domain only constructs: WT, with mutation S121R or A123S. The intracellular (I), secreted (S) and ECM (M) fractions were collected and HTRA1 was detected by anti-V5 immunoblot. A: Image representative of 2 independent assays. B: One assay among several was selected, based on the ECM insertion of WT HTRA1.

To conclude, my data suggest that the Mac-domain mediates the insertion of HTRA1 in the ECM. I further identify vitronectin and fibronectin as putative ECM partners of HTRA1. However, Mac-domain mutations seem not to alter the deposition of HTRA1 in the ECM.

7 - Discussion

Over the past years, the number of mono- and biallelic *HTRA1* mutations identified in CSVD cases has risen steadily. Besides archetypal loss-of-function mutations, missense mutations within the HTRA1 Mac-domain constitute an emerging but poorly investigated subgroup which are examined within this thesis.

7.1 - Missense mutations within the Kazal-like domain cause a mild CSVD phenotype

Six distinct missense Mac-domain mutations have been reported in seven unrelated heterozygous probands manifesting with familial CSVD. These rare genetic variants are predicted to affect protein function and/or to be disease causing by multiple independent *in silico* tools. Moreover, they cluster in the carboxyterminal Kazal-domain of the Mac-domain. In fact, reported to the size of the distinct HTRA1 domains, CSVD-related missense mutations within the Kazal-domain appear as frequent as the classical protease-domain mutations, whereas missense mutations rarely target the IGFBP- or PDZ-domain. Still, since the genotype/phenotype correlation within the affected families has not been addressed, the pathogenicity of missense Mac-domain mutations remains unclear [27, 62, 63]. This is strengthened by the facts that (i) the function of the Mac-domain, which is dispensable for protease activity, is unknown [54], (ii) Mac-domain mutations seem not to interfere with the enzymatic activity of HTRA1 *in vitro* ([94]; ISD, unpublished observations) and (iii) alternative loss-of-function mechanisms have not been reported. Hence there is a lack of evidence whether and how these mutations alter HTRA1 function.

Based on literature-analysis, the demographic information and clinical phenotype of symptomatic cases bearing heterozygous Mac-domain mutations (n = 7) to that of heterozygous patients bearing archetypical HTRA1 loss-of-function mutations (n = 56) were compared. While both patient subgroups exhibit classical CSVD features, Mac-domain mutation carriers tend to include less males. Importantly, the occurrence of both severe neurological (*i.e.*, stroke) and extraneurological manifestations (such as spondylosis and alopecia) seem to be less frequent. Future analyses on larger samples are required to clarify this possibility. Of note, comparison of neuroimaging features such as WMH severity, as well as the presence or absence of lacunes and microbleeds, is hampered by the lack of well-defined, universal MRI criteria across centers. Collectively, despite the small number of Mac-domain mutation carriers and

heterogeneity in the quality of case-reports and cohort-studies, especially in the recording of extraneurological manifestations and neuroimaging features, my observations suggest that Mac-domain mutations cause a distinct, milder CSVD (with fewer strokes and extraneurological symptoms.)

7.2 - Putative loss-of-function mechanisms linked to HTRA1 Mac-domain mutations

Various molecular and/or cellular mechanisms might underlie the pathogenicity of Mac-domain mutations (**Figure 19**) [110, 111].
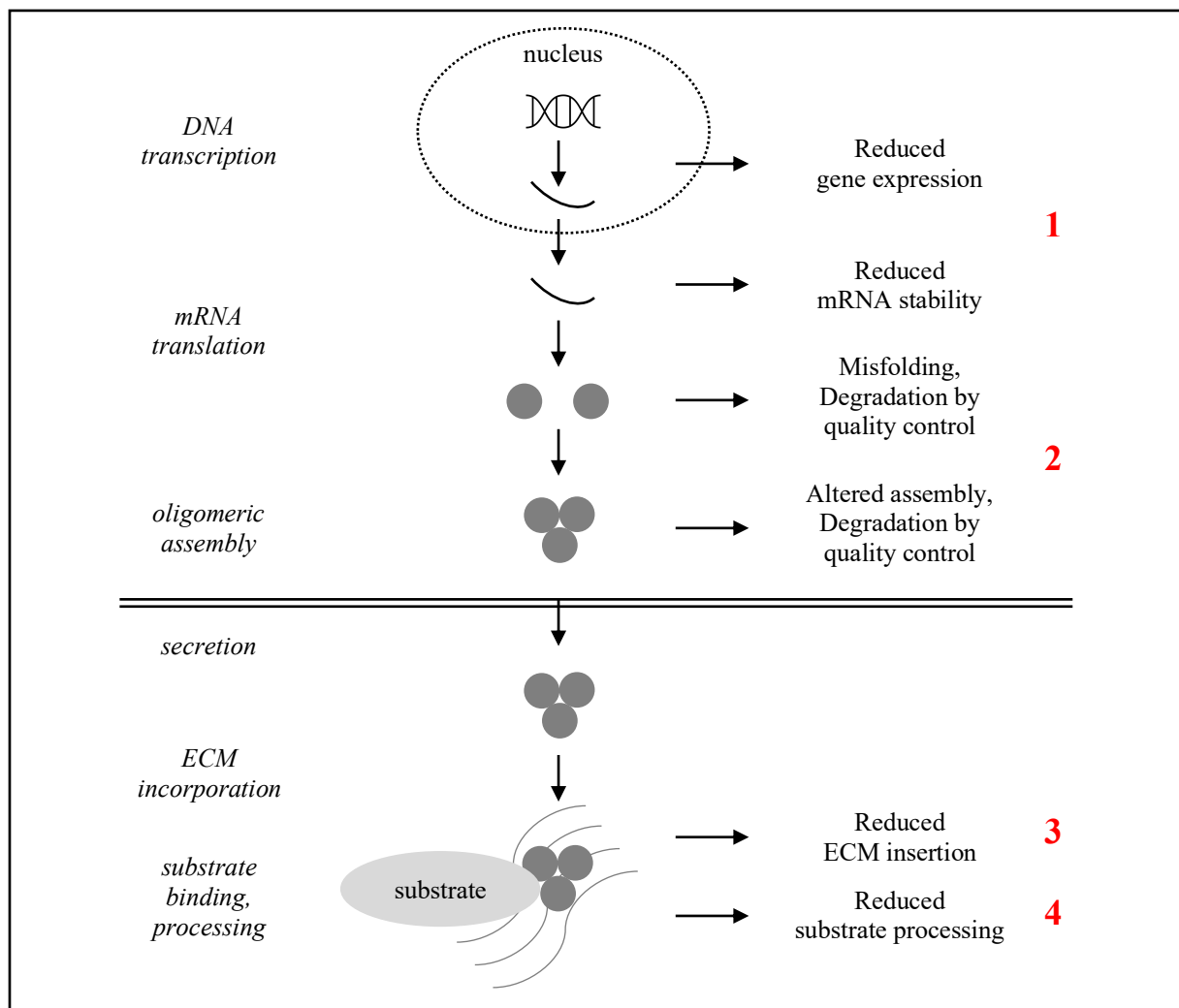
Figure 19: Putative molecular and cellular mechanisms underlying HTRA1 loss-of-function caused by Mac-domain missense mutations.

An array of mechanisms might underly Mac-domain mutations-related HTRA1 loss-of-function. First, mutations might alter *HTRA*1 gene expression and/or mRNA stability. Second, they could interfere with HTRA1 protein folding and conformation (including its multimeric assembly), possibly reducing its intrinsic stability and/or promoting its degradation by the protein quality control systems. If secreted, Mac-domain HTRA1 mutants might exhibit a reduced affinity for the ECM or for discrete substrates. Numbers (1-4) correspond to features discussed in the text.

7.2.1 - *HTRA1* gene expression and mRNA stability

HTRA1 mutations, including mutations linked to amino acid variation such as the missense Mac-domain mutations, can in principle exert their deleterious effects via the consequence of the nucleotide variation on transcription, splicing and/or mRNA stability. This has been well documented for mutation R370X [26]. Indeed, analysis of patient skin fibroblasts revealed that 1108C>T/R370X causes nonsense-mediated mRNA decay, thereby reducing HTRA1 protein levels and function [26]. Conversely, when recombinantly expressed and tested, R370X protein exhibits a normal protease activity. Besides the specific case of nonsense-mediated mRNA decay, many examples have shown that missense mutations can affect mRNA levels by modifying *e.g.*, a promoter enhancer/repressor or a splicing regulatory element [111]. These aspects were not addressed in the present study, as patient material was not available. Meanwhile, HTRA1 mRNA and protein levels have been reported to be reduced in cultured skin fibroblasts derived from a heterozygous individual carrying the missense Mac-domain mutation Q151K [112], pinpointing the relevance of such assays. To overcome the rarity of patient material and evaluate the impact of HTRA1 mutation in vascular cells, future assays could take advantage of the tremendous progresses in the field of CRISPR/Cas9-mediated genome editing of pluripotent stem cells (iPSC) [113].

7.2.2 - HTRA1 protein conformation and stability

Aberrant proteins, characterized by *e.g.*, folding or oligomeric assembly defects, are typically degraded by the ubiquitin-proteasome system or by autophagy [114, 115]. For instance, a set of pathogenic mutations in the Kazal-domain of the trypsin inhibitor SPINK1, has been reported to cause intracellular retention and degradation of the corresponding mutant proteins [116]. Thus, I tested whether missense Mac-domain mutations exhibit an abnormal conformation and/or undergo intracellular retention and degradation as a mechanism underlying loss-of-function (**Figure 19**). Using purified proteins, I observed that a distinct Mac-domain mutant (S121R) indeed displays an increased resistance to trypsin digestion and exists as a monomer/dimer/trimer mixture, compared to the almost complete trimeric assembly of control HTRA1. Both results indicate conformational defects (possibly partial misfolding). Accordingly, this mutant also displays a reduced intracellular stability in overexpressing HEK-293T cells indicating that it either exhibits a reduced intrinsic stability, or that it is detected and erased by the cell quality control machinery. Conversely, the other mutants assessed showed normal intracellular stability. However, overexpression poses methodological limitations, as

the quality control systems might be overloaded by the large amount of recombinant HTRA1. Future assays might thus evaluate the behavior of endogenous HTRA1, using *e.g.*, patient skin fibroblasts (if available) or CRISPR/Cas9 edited cell lines (see above). In addition, further assays should characterize the proteostasis of S121R. In particular, the respective contribution of the ubiquitin-proteasome system and of autophagy to the degradation of this unstable mutant could be assessed *e.g.*, using selective inhibitors.

7.2.3 - ECM insertion of HTRA1

Recent evidence from genetics and analysis of experimental models pinpoints perturbation of the cerebrovascular matrisome as a key feature in SVD [50, 117]. Regarding HTRA1, this is exemplified by the facts that the protein (i) is present in the ECM both in cell cultures and in vascular tissues [84, 85] and (ii) regulates the bioavailability of the matrix-associated growth factor TGF-beta via limited cleavage of its ligand LTBP1 [84], while (iii) HTRA1 deficiency is linked to a marked cerebrovascular accumulation of matrisomal proteins [17]. Conceivably, the association of HTRA1 with the ECM might facilitate the processing of its matrisomal targets via local co-enrichment of the protease and its substrates. Therefore, the association of HTRA1 with the ECM was investigated. Using truncated HTRA1 constructs, and sequential protein extraction followed by immunoblot, the Mac-domain was found to be essential for the insertion of HTRA1 in the ECM of cultured fibroblasts. Of importance, this thesis provides the first description of a Mac-domain-related function. Using a limited set of purified ECM proteins and a solid-phase binding assay, vitronectin and fibronectin were identified as putative matrisomal HTRA1 interactants. However, there was no indication that Mac-domain mutations interfere with the ECM integration of HTRA1. Still, since the ECM produced by fibroblasts in culture diverges from that of vascular cells, further experiments should evaluate the association of HTRA1 in general and of the Mac-domain mutants in particular with the ECM produced by, *e.g.*, cultured endothelial cells (at best brain endothelial cells) and smooth muscle cells. In addition, high-throughput methods involving *e.g.*, the recombinant overexpression of HTRA1 Mac-domain in vascular cells followed by pull-down and mass spectrometry-based identification of the bound proteins could be applied to identify the vessel-relevant matrisomal ligands of the Mac-domain.

7.2.4 - HTRA1 protease activity

So far, activity assays using Mac-domain mutants had been restricted to measurement of the degradation of analytical substrates such as casein and BSA by recombinant HTRA1 ([94]; ISD, unpublished observations). Such assays indicated that Mac-domain mutations do not alter the enzymatic activity of HTRA1. Since binding of the substrate to the protease represents the initial step of the proteolytic reaction, I tested whether Mac-domain mutants might display a reduced activity towards HTRA1 physiological substrates such as fibronectin and LTBP1. Although no difference in enzymatic activity was observed for Mac-domain mutants compared to HTRA1 WT, further assays should evaluate additional targets. In particular, LTBP4 and PRSS23 (serine protease 23) represent promising candidates since my host laboratory recently (i) demonstrated that both proteins are cleaved by HTRA1 *in vitro* and (ii) proved that HTRA1 loss-of-function alters their cleavage pattern *in vivo* and *in situ* in the brain vasculature of HTRA1 mutant mice (ISD, unpublished results).

Of note, based on the analysis of archetypal HTRA1 mutations, HTRA1-related CSVD is postulated to result from HTRA1 loss-of-function [26]. However, the possibility that Mac-domain mutations involve a gain-of-function in HTRA1 should not be fully excluded. Indeed, as seen for *e.g.*, TGF-beta [118], vascular homeostasis relies on the fine-tune control of bioactive mediators. Specifically, while loss of HTRA1 function is detrimental to the brain vasculature, elevated levels and activity might also damage brain vessels as seen in the retina of HTRA1 overexpressing mice [119] and of age-related macular degeneration cases [120].

In conclusion, my work suggests that Mac-domain mutations which cluster within the Kazal-domain might cause a milder CSVD than archetypal HTRA1 loss-of-function mutations. Although my data do not elucidate a common loss-of-function mechanism, I provide evidence that S121R affects the conformation and stability of HTRA1. On another note, my results point to a role of the Mac-domain in mediating the incorporation of HTRA1 in the ECM.

A - Supplementary

The following **Supplementary Figure 1** summarizes the reported family trees of HTRA1 Mac-domain mutation carriers. Additionally, **Supplementary Table 1** provides an overview on the phenotypes of archetypical heterozygous HTRA1 mutation carriers, served for the phenotype comparison in **Section 6.1.1**.
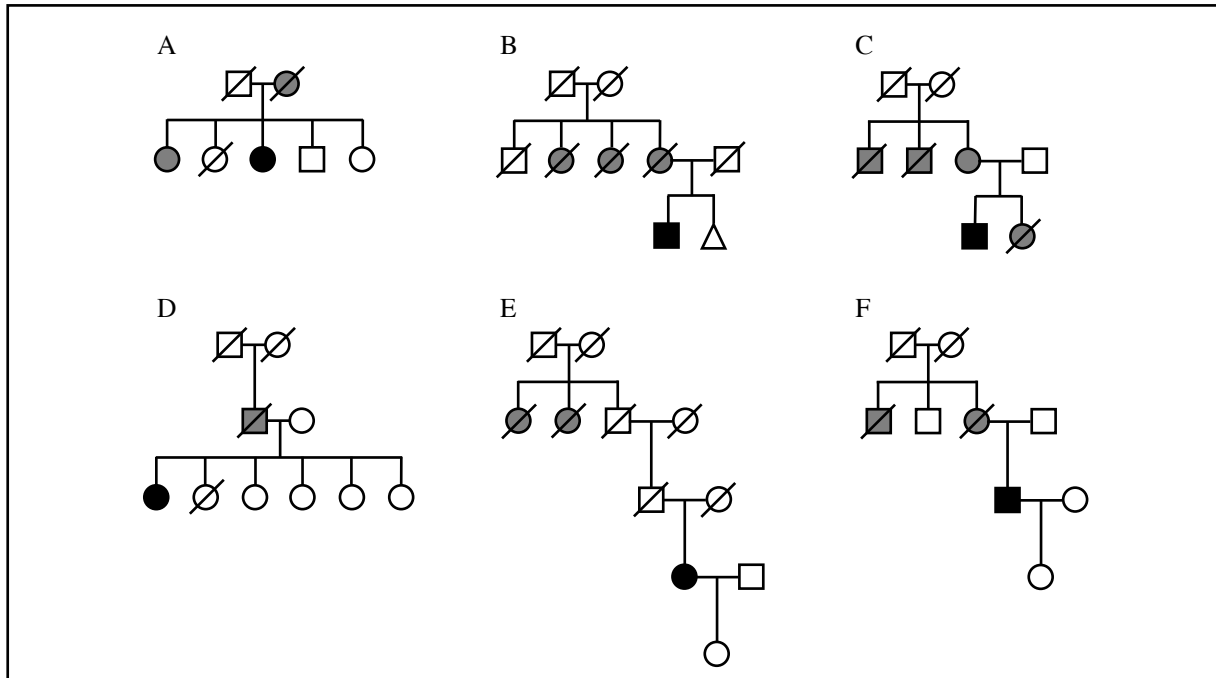
Supplementary Figure 120: Family trees of HTRA1 Mac-domain mutation carriers.
Family trees of following HTRA1 Mac-domain mutation carriers: A: G120D, B: S121R, C: A123S, D: A133G, E: S136G, F: Q151K. Circle = female; square = male; triangle = pregnancy; diagonal line = deceased; grey symbols = neurologically affected relatives according to family history; filled symbols = reported index patient with genetically proven heterozygous HTRA1 mutation. (A based on [64]; B, C, D based on [27]; E, F based on [63]).

Missense mutations within HTRA1 protease-domain

Mutation	Family	Gender	AO	Initial symptom	AD	AHT	Stroke; TIA	CI	Dementia	Gait disturbance	Alopecia	Psychiatric disorder	Spondylosis	Any (additional) (extra-)neurological disease/ manifestation, vascular RF, course of disease	WMH	Lacunes	Micro-bleeds	Age	Reference
				General					Main neurological manifestations		Extraneurological CARASIL manifestations			Manifestation		Neuroimaging			
p.Arg166Leu	F1	M	66	CI; (lumbar disk prolapse)	69	0	1	1	0	1	0	1	1	hypercholesterolaemia	1	1	0	69	[27]
		M	55	depression	64	0	0	1	0	0	0	1	0	arthritis	1	0	0	NA	
		F	60	CI	65	AHT	1	1	0	0	0	0	0	hypercholesterolaemia	1	1	1	NA	
p.Arg166Cys	F1	M	41	CI, mood lability	43	0	0	1	0	1	0	1	0	vitiligo, autoimmune hyperthyroidism, smoking	1	1	1	43	[121]
		M	45	CI	47	0	1	1	0	0	0	0	0	0	1	1	0	47	
		M	29	migraine	31	0	0	1	0	0	1	0	0	hearing loss	1	NA	0	NA	[122]
		F	35	S	38	NA	1	1	0	1	1	1	1	urinary incontinence	1	1	1	NA	[66]
	F2	M	71	vertigo, gait distrubance	77	0	1	1	1	1	0	1	0	0	1	1	0	NA	[123]
		M	53	dysarthria, dysphasia	56	AHT	1	1	0	1	0	1	0	died hyperlipidemia	1	1	0	56	
p.Ala173Pro		F	65	balance impairment	72	AHT	0	1	0	1	0	NA	0	NA	1	1	NA	72	[27]
p.Val175Met		M	59	gait disturbance (TIA, CI)	77	AHT	1	1	0	1	NA	NA	NA	died, dyslipidemia	1	1	NA	NA	[63]
		M	49	S	54	AHT	1	1	0	0	1	1	1	urinary incontinence, diabetes mellitus	1	1	1	NA	[66]
p.Val176Ala	F1	M	64	S	71	AHT	1	1	1	1	1	1	0	bedridden, quadriplegia, incontinence	1	1	1	NA	[124]
		M	77	S	84	AHT	1	NA	NA	NA	1	NA	NA	1	NA	NA	NA	NA	
		M	70	S	82	NA	1	NA	NA	1	1	NA	NA	bedridden	NA	NA	NA	NA	
		M	63	S	66	NA	1	NA	NA	NA	NA	NA	NA	NA	1	1	1	66	
		M	61	S	63	NA	1	NA	NA	NA	NA	NA	NA	NA	1	1	0	63	
p.Ile179Asn	F1	M	48	TIA	48	AHT	1	0	0	0	0	0	1	dyslipidemia coronary artery disease	1	1	0	50	[64]
		F	46	episodic hemicrania	48	0	1	0	0	0	0	0	0	0	1	1	0	48	
p.Ser205Cys	F1	F	46	CI	53	0	1	1	0	0	0	1	0	0	1	1	NA	NA	[125]
		F	47	low back pain, headache	60	0	0	1	0	0	0	1	1	0	1	1	NA	60	
p.Gly206Glu		M	55	gait disturbance	65	AHT	0	1	0	1	0	1	0	0	1	NA	NA	NA	[63]
p.Val216Met	F1	M	48	gait disturbance	48	AHT	1	1	0	1	1	1	1	dyslipidemia smoking	1	1	1	48	[126]
		M	52	S	52	AHT	1	0	0	0	1	0	1	dyslipidemia diabetes mellitus	1	0	0	52	
p.Ile256Thr		M	54	CI	60	AHT	0	1	1	0	0	1	1	0	1	1	NA	60	[64]
p.Gly276Ala		F	49	S	56	0	1	1	0	1	0	1	1	dyslipidemia	1	1	1	56	[64]
p.Gly283Glu		M	49	CI, gait disturbance	49	0	0	1	0	1	0	NA	1	died, alcohol abuse, smoking	1	NA	NA	NA	[62]

Mutation	Family	Sex	AO	Clinical manifestation	AD	AHT								Comorbidities / outcome				Age	Ref
p.Gly283Arg		M	32	gait disturbance, weak limbness	39	0	1	1	0	1	0	NA	1	died, urinary incontinence, seizures	1	1	NA	39	[127]
p.Ser284Arg		F	NA	Headaches	49	AHT	0	0	0	0	NA	NA	NA	NA	1	1	0	49	[27]
p.Ser284Gly		F	62	S	62	0	1	0	0	0	NA	NA	NA	NA	1	1	1	62	[27]
p.Pro285Gln		M	50	S	55	0	1	0	0	1	NA	NA	NA	NA	1	1	NA	50	[27]
p.Pro285Leu		M	32	S gait disturbance	51	AHT	1	1	0	1	1	NA	1	0	1	1	1	51	[62]
		M	51	S	59	0	1	1	0	1	0	NA	1	smoking	1	NA	NA	59	[62]
		M	63	gait disturbance	65	NA	NA	NA	NA	1	1	0	0	0	NA	NA	NA	NA	[128]
p.Phe286Val		M	49	S	55	0	1	1	0	1	NA	NA	NA	NA	1	1	NA	55	[27]
p.Gly295Arg	F1	M	65	CI	73	0	0	1	0	1	0	1	0	bedridden	1	NA	NA	NA	[63]
		M	67	CI, TIA	71	AHT	1	1	0	0	0	1	0	0	1	1	NA	67	[63]
p.Val297Met		M	44	migraine	56	AHT	0	1	0	0	0	0	0	sensory and autonomic small fiber neuropathy	1	NA	1	54	[129]
p.Arg302Gln	F1	M	63	S, CI, gait disturbance	63	AHT	1	1	0	1	0	NA	1	smoking	1	NA	NA	63	[62]
		M	40	CI, gait disturbance	57	0	0	1	0	1	1	NA	1	alcohol abuse	1	NA	NA	57	[62]
	F2	M	44	CI	61	0	0	1	0	1	1	NA	1	alcohol abuse, smoking	1	1	1	61	[62]
		M	57	CI	60	0	1	1	0	1	0	NA	1	smoking	1	NA	NA	NA	[62]
	F3	M	55	CI	55	0	1	1	1	0	0	0	1	died, follicular lymphoma, secondary myelodasplastic syndrome	1	0	1	55	[61]
		M	44	CI	NA	NA	NA	NA	1	NA	NA	NA	NA	NA	1	NA	NA	NA	NA
	F4	M	35	dizziness, limb weakness	NA	0	1	1	0	0	NA	NA	NA	0	1	1	NA	NA	[130]
		F	48	Recurrent S	63	0	1	1	0	0	NA	NA	NA	0	1	1	NA	NA	[130]
p.Thr319Ile		M	53	S, CI, gait disturbance	57	AHT	1	1	0	1	0	NA	1	dyslipidemia	1	NA	NA	NA	[62]
p.Asn324Thr		M	60	limb weakness	65	0	1	1	0	1	0	0	1	0	1	1	NA	65	[64]
		F	37	S	40	0	1	1	0	1	0	1	0	0	1	1	1	40	[66]
HTRA1 nonsense, frameshift and intronic mutation before catalytic Ser^{328}																			
p.Gln151*		F	29	S	63	AHT	1	0	0	1	0	1	1	urinary incontinence	1	1	1	NA	[131]
p.Ala182fs*33		M	62	dizziness, gait disturbance	65	AHT	1	1	0	1	0	1	1	died, smoking	1	1	1	64	[64]
p.Arg197*		M	77	S	78	AHT	1	1	1	NA	NA	NA	NA	0	1	1	NA	NA	[124]
p.Glu277fs		M	NA	S	57	AHT	1	0	0	0	NA	NA	NA	died	NA	NA	NA	NA	[132]
p.Glu289Ter	F1	F	55	S	64	0	1	1	0	0	1	1	1	0	1	1	1	NA	[64]
		M	66	gait disturbance	68	0	0	0	0	1	1	0	1	alcohol abuse	1	1	0	68	[64]
p.Arg302Ter		M	59	S	63	0	1	1	0	1	0	0	0	0	1	1	1	NA	[133]

Supplementary Table 11: Archetypal HTRA1 mutations linked to CSVD.
Patients with missense mutations within HTRA1 protease-domain and HTRA1 nonsense, frameshift and intronic mutation before catalytic Ser^{328} reported until December 31, 2020 are listed. Patients who were eligible based on the clinical picture but were not genetically confirmed were not included, nor were patients who, despite detection of a heterozygous HTRA1 mutation, had no report or no neurological manifestations. Patients with any additional known mutation in a gene associated with neurovascular disease were excluded. There are major differences in the literature regarding the presentation of individual cases and the neuroradiological assessment of corresponding MRI images. Abbreviations used: 1 = present, 0 = absent, AD = age of diagnosis, AHT = arterial hypertension, AO = age of onset, CI = cognitive impairment, F = female, F1/F2/F3/F4 = different families, M = male, NA = not available, S = stroke, TIA = transient ischemic attack.

B - Copyright declaration

Figure 2E has been published [58] by Blackwell Publishing (John Wiley & Sons – Journals) under a creative commons license (CC BY-NC-ND 4.0) [11]. **Copyright declaration Table 1** lists the license numbers for the reproduction of the additional figures obtained through RightsLink[12].

Figure	Reference	Publisher	Rightsholder	License number
1A	[2]	Lancet Publishing Group	Elsevier Science & Technology Journals	1198785-1
1B	[3]	Lancet Publishing Group	Elsevier Science & Technology Journals	1198785-2
1C	[1]	Lancet Publishing Group	Elsevier Science & Technology Journals	1198785-3
2B; 2D	[56]	Dr Dietrich Steinkopff Verlag	Springer	1198785-4
2C	[57]	W.B. Saunders Co.	Elsevier Science & Technology Journals	1198785-5
2F; 2G	[59]	Blackwell Publishing	John Wiley & Sons - Journals	1198785-6
3B	[27]	Oxford University Press	Oxford University Press - Journals	1198785-7
3C; 3D	[61]	Blackwell Publishing Asia	John Wiley & Sons - Journals	1198785-8
5A	[54]	Cell Press	Elsevier Science & Technology Journals	1262503-1

Copyright declaration Table 12: License numbers for reproducing published figures.

---

[11] https://creativecommons.org/licenses/by-nc-nd/4.0/
[12] https://www.copyright.com/publishers/rightslink-permissions/

C - Bibliography

1.   Pantoni, L., *Cerebral small vessel disease: from pathogenesis and clinical characteristics to therapeutic challenges.* Lancet Neurol, 2010. **9**(7): p. 689-701.
2.   Wardlaw, J.M., C. Smith, and M. Dichgans, *Small vessel disease: mechanisms and clinical implications.* Lancet Neurol, 2019. **18**(7): p. 684-696.
3.   Wardlaw, J.M., C. Smith, and M. Dichgans, *Mechanisms of sporadic cerebral small vessel disease: insights from neuroimaging.* Lancet Neurol, 2013. **12**(5): p. 483-97.
4.   Fisher, C.M., *Lacunar strokes and infarcts: a review.* Neurology, 1982. **32**(8): p. 871-6.
5.   Wardlaw, J.M., et al., *Neuroimaging standards for research into small vessel disease and its contribution to ageing and neurodegeneration.* Lancet Neurol, 2013. **12**(8): p. 822-38.
6.   Marini, S., C.D. Anderson, and J. Rosand, *Genetics of Cerebral Small Vessel Disease.* Stroke, 2020. **51**(1): p. 12-20.
7.   Collaborators, G.B.D.N., *Global, regional, and national burden of neurological disorders, 1990-2016: a systematic analysis for the Global Burden of Disease Study 2016.* Lancet Neurol, 2019. **18**(5): p. 459-480.
8.   Wolters, F.J. and M.A. Ikram, *Epidemiology of Vascular Dementia.* Arterioscler Thromb Vasc Biol, 2019. **39**(8): p. 1542-1549.
9.   Kapasi, A., C. DeCarli, and J.A. Schneider, *Impact of multiple pathologies on the threshold for clinically overt dementia.* Acta Neuropathol, 2017. **134**(2): p. 171-186.
10.   Pasi, M. and C. Cordonnier, *Clinical Relevance of Cerebral Small Vessel Diseases.* Stroke, 2020. **51**(1): p. 47-53.
11.   van der Holst, H.M., et al., *White matter changes and gait decline in cerebral small vessel disease.* Neuroimage Clin, 2018. **17**: p. 731-738.
12.   Group, L.S., *2001-2011: a decade of the LADIS (Leukoaraiosis And DISability) Study: what have we learned about white matter changes and small-vessel disease?* Cerebrovasc Dis, 2011. **32**(6): p. 577-88.
13.   Rensma, S.P., et al., *Cerebral small vessel disease and risk of incident stroke, dementia and depression, and all-cause mortality: A systematic review and meta-analysis.* Neurosci Biobehav Rev, 2018. **90**: p. 164-173.
14.   de Leeuw, F.E., et al., *Prevalence of cerebral white matter lesions in elderly people: a population based magnetic resonance imaging study. The Rotterdam Scan Study.* J Neurol Neurosurg Psychiatry, 2001. **70**(1): p. 9-14.
15.   Hilal, S., et al., *Prevalence, risk factors and consequences of cerebral small vessel diseases: data from three Asian countries.* J Neurol Neurosurg Psychiatry, 2017. **88**(8): p. 669-674.
16.   Cannistraro, R.J., et al., *CNS small vessel disease: A clinical review.* Neurology, 2019. **92**(24): p. 1146-1156.
17.   Zellner, A., et al., *CADASIL brain vessels show a HTRA1 loss-of-function profile.* Acta Neuropathol, 2018. **136**(1): p. 111-125.
18.   Mancuso, M., et al., *Monogenic cerebral small-vessel diseases: diagnosis and therapy. Consensus recommendations of the European Academy of Neurology.* Eur J Neurol, 2020. **27**(6): p. 909-927.
19.   Prins, N.D. and P. Scheltens, *White matter hyperintensities, cognitive impairment and dementia: an update.* Nat Rev Neurol, 2015. **11**(3): p. 157-65.
20.   Ter Telgte, A., et al., *Cerebral small vessel disease: from a focal to a global perspective.* Nat Rev Neurol, 2018. **14**(7): p. 387-398.

21. Ji, T., et al., *Effect of Low-Dose Statins and Apolipoprotein E Genotype on Cerebral Small Vessel Disease in Older Hypertensive Patients: A Subgroup Analysis of a Randomized Clinical Trial.* J Am Med Dir Assoc, 2018. **19**(11): p. 995-1002 e4.

22. Kwok, C.S., et al., *Efficacy of antiplatelet therapy in secondary prevention following lacunar stroke: pooled analysis of randomized trials.* Stroke, 2015. **46**(4): p. 1014-23.

23. French, C.R., et al., *Mutation of FOXC1 and PITX2 induces cerebral small-vessel disease.* J Clin Invest, 2014. **124**(11): p. 4877-81.

24. Tournier-Lasserve, E., et al., *Cerebral autosomal dominant arteriopathy with subcortical infarcts and leukoencephalopathy maps to chromosome 19q12.* Nat Genet, 1993. **3**(3): p. 256-9.

25. Bugiani, M., et al., *Cathepsin A-related arteriopathy with strokes and leukoencephalopathy (CARASAL).* Neurology, 2016. **87**(17): p. 1777-1786.

26. Hara, K., et al., *Association of HTRA1 mutations and familial ischemic cerebral small-vessel disease.* N Engl J Med, 2009. **360**(17): p. 1729-39.

27. Verdura, E., et al., *Heterozygous HTRA1 mutations are associated with autosomal dominant cerebral small vessel disease.* Brain, 2015. **138**(Pt 8): p. 2347-58.

28. Favor, J., et al., *Type IV procollagen missense mutations associated with defects of the eye, vascular stability, the brain, kidney function and embryonic or postnatal viability in the mouse, Mus musculus: an extension of the Col4a1 allelic series and the identification of the first two Col4a2 mutant alleles.* Genetics, 2007. **175**(2): p. 725-36.

29. Ding, X.Q., et al., *MRI features of pontine autosomal dominant microangiopathy and leukoencephalopathy (PADMAL).* J Neuroimaging, 2010. **20**(2): p. 134-40.

30. Verdura, E., et al., *Disruption of a miR-29 binding site leading to COL4A1 upregulation causes pontine autosomal dominant microangiopathy with leukoencephalopathy.* Ann Neurol, 2016. **80**(5): p. 741-753.

31. Siitonen, M., et al., *Multi-infarct dementia of Swedish type is caused by a 3'UTR mutation of COL4A1.* Brain, 2017. **140**(5): p. e29.

32. Zhou, Q., et al., *Early-onset stroke and vasculopathy associated with mutations in ADA2.* N Engl J Med, 2014. **370**(10): p. 911-20.

33. Kint, J.A., *Fabry's disease: alpha-galactosidase deficiency.* Science, 1970. **167**(3922): p. 1268-9.

34. Desnick, R.J., et al., *Fabry disease: molecular diagnosis of hemizygotes and heterozygotes.* Enzyme, 1987. **38**(1-4): p. 54-64.

35. Wattendorff, A.R., et al., *Familial cerebral amyloid angiopathy presenting as recurrent cerebral haemorrhage.* J Neurol Sci, 1982. **55**(2): p. 121-35.

36. Van Broeckhoven, C., et al., *Amyloid beta protein precursor gene and hereditary cerebral hemorrhage with amyloidosis (Dutch).* Science, 1990. **248**(4959): p. 1120-2.

37. Mandybur, T.I. and S.R. Bates, *Fatal massive intracerebral hemorrhage complicating cerebral amyloid angiopathy.* Arch Neurol, 1978. **35**(4): p. 246-8.

38. Ghiso, J., O. Jensson, and B. Frangione, *Amyloid fibrils in hereditary cerebral hemorrhage with amyloidosis of Icelandic type is a variant of gamma-trace basic protein (cystatin C).* Proc Natl Acad Sci U S A, 1986. **83**(9): p. 2974-8.

39. Verreault, S., et al., *A novel hereditary small vessel disease of the brain.* Ann Neurol, 2006. **59**(2): p. 353-7.

40. Munke, M., et al., *The gene for cystathionine beta-synthase (CBS) maps to the subtelomeric region on human chromosome 21q and to proximal mouse chromosome 17.* Am J Hum Genet, 1988. **42**(4): p. 550-9.

41. Harpey, J.P., et al., *Homocystinuria caused by 5,10-methylenetetrahydrofolate reductase deficiency: a case in an infant responding to methionine, folinic acid, pyridoxine, and vitamin B12 therapy.* J Pediatr, 1981. **98**(2): p. 275-8.

42. Smahi, A., et al., *Genomic rearrangement in NEMO impairs NF-kappaB activation and is a cause of incontinentia pigmenti. The International Incontinentia Pigmenti (IP) Consortium.* Nature, 2000. **405**(6785): p. 466-72.

43. Pavlakis, S.G., et al., *Mitochondrial myopathy, encephalopathy, lactic acidosis, and strokelike episodes: a distinctive clinical syndrome.* Ann Neurol, 1984. **16**(4): p. 481-8.

44. Deschauer, M., et al., *MELAS associated with mutations in the POLG1 gene.* Neurology, 2007. **68**(20): p. 1741-2.

45. Kavanagh, D., et al., *New roles for the major human 3'-5' exonuclease TREX1 in human disease.* Cell Cycle, 2008. **7**(12): p. 1718-25.

46. Neel, J.V., *The Inheritance of Sickle Cell Anemia.* Science, 1949. **110**(2846): p. 64-6.

47. Rannikmae, K., et al., *Beyond the Brain: Systematic Review of Extracerebral Phenotypes Associated With Monogenic Cerebral Small Vessel Disease.* Stroke, 2020. **51**(10): p. 3007-3017.

48. Narayan, S.K., et al., *The minimum prevalence of CADASIL in northeast England.* Neurology, 2012. **78**(13): p. 1025-7.

49. van der Tol, L., et al., *A systematic review on screening for Fabry disease: prevalence of individuals with genetic variants of unknown significance.* J Med Genet, 2014. **51**(1): p. 1-9.

50. Joutel, A., et al., *Perturbations of the cerebrovascular matrisome: A convergent mechanism in small vessel disease of the brain?* J Cereb Blood Flow Metab, 2016. **36**(1): p. 143-57.

51. Malik, R., et al., *Multiancestry genome-wide association study of 520,000 subjects identifies 32 loci associated with stroke and stroke subtypes.* Nat Genet, 2018. **50**(4): p. 524-537.

52. Rannikmae, K., et al., *Common variation in COL4A1/COL4A2 is associated with sporadic cerebral small vessel disease.* Neurology, 2015. **84**(9): p. 918-26.

53. Schmidt, H., et al., *Genetic variants of the NOTCH3 gene in the elderly and magnetic resonance imaging correlates of age-related cerebral small vessel disease.* Brain, 2011. **134**(Pt 11): p. 3384-97.

54. Eigenbrot, C., et al., *Structural and functional analysis of HtrA1 and its subdomains.* Structure, 2012. **20**(6): p. 1040-50.

55. Maeda, S., et al., *Familial unusual encephalopathy of Binswanger's type without hypertension.* Folia Psychiatr Neurol Jpn, 1976. **30**(2): p. 165-77.

56. Khaleeli, Z., et al., *A novel HTRA1 exon 2 mutation causes loss of protease activity in a Pakistani CARASIL patient.* J Neurol, 2015. **262**(5): p. 1369-72.

57. Fukutake, T., *Cerebral autosomal recessive arteriopathy with subcortical infarcts and leukoencephalopathy (CARASIL): from discovery to gene identification.* J Stroke Cerebrovasc Dis, 2011. **20**(2): p. 85-93.

58. Tikka, S., et al., *CADASIL and CARASIL.* Brain Pathol, 2014. **24**(5): p. 525-44.

59. Oide, T., et al., *Extensive loss of arterial medial smooth muscle cells and mural extracellular matrix in cerebral autosomal recessive arteriopathy with subcortical infarcts and leukoencephalopathy (CARASIL).* Neuropathology, 2008. **28**(2): p. 132-42.

60. Uemura, M., et al., *HTRA1-Related Cerebral Small Vessel Disease: A Review of the Literature.* Front Neurol, 2020. **11**: p. 545.

61. Ito, J., et al., *Histopathologic features of an autopsied patient with cerebral small vessel disease and a heterozygous HTRA1 mutation.* Neuropathology, 2018.

62. Nozaki, H., et al., *Distinct molecular mechanisms of HTRA1 mutants in manifesting heterozygotes with CARASIL.* Neurology, 2016. **86**(21): p. 1964-74.

63.   Di Donato, I., et al., *Heterozygous mutations of HTRA1 gene in patients with familial cerebral small vessel disease.* CNS Neurosci Ther, 2017. **23**(9): p. 759-765.

64.   Lee, Y.C., et al., *Characterization of Heterozygous HTRA1 Mutations in Taiwanese Patients With Cerebral Small Vessel Disease.* Stroke, 2018. **49**(7): p. 1593-1601.

65.   Tan, R.Y.Y., et al., *How common are single gene mutations as a cause for lacunar stroke? A targeted gene panel study.* Neurology, 2019. **93**(22): p. e2007-e2020.

66.   Liu, J.Y., et al., *HTRA1-related autosomal dominant cerebral small vessel disease.* Chin Med J (Engl), 2020.

67.   Rannikmae, K., et al., *COL4A2 is associated with lacunar ischemic stroke and deep ICH: Meta-analyses among 21,500 cases and 40,600 controls.* Neurology, 2017. **89**(17): p. 1829-1839.

68.   Sargurupremraj, M., et al., *Cerebral small vessel disease genomics and its implications across the lifespan.* Nat Commun, 2020. **11**(1): p. 6285.

69.   Mishra, A., et al., *Association of variants in HTRA1 and NOTCH3 with MRI-defined extremes of cerebral small vessel disease in older subjects.* Brain, 2019. **142**(4): p. 1009-1023.

70.   Liu, G., et al., *Rs2293871 regulates HTRA1 expression and affects cerebral small vessel stroke and Alzheimer's disease.* Brain, 2019. **142**(11): p. e61.

71.   Clausen, T., C. Southan, and M. Ehrmann, *The HtrA family of proteases: implications for protein composition and cell fate.* Mol Cell, 2002. **10**(3): p. 443-55.

72.   Zurawa-Janicka, D., et al., *Structural insights into the activation mechanisms of human HtrA serine proteases.* Arch Biochem Biophys, 2017. **621**: p. 6-23.

73.   Risor, M.W., et al., *The autolysis of human HtrA1 is governed by the redox state of its N-terminal domain.* Biochemistry, 2014. **53**(23): p. 3851-7.

74.   Zumbrunn, J. and B. Trueb, *Primary structure of a putative serine protease specific for IGF-binding proteins.* FEBS Lett, 1996. **398**(2-3): p. 187-92.

75.   Goettig, P., H. Brandstetter, and V. Magdolen, *Surface loops of trypsin-like serine proteases as determinants of function.* Biochimie, 2019. **166**: p. 52-76.

76.   Lorenzi, T., et al., *HtrA1 in human urothelial bladder cancer: a secreted protein and a potential novel biomarker.* Int J Cancer, 2013. **133**(11): p. 2650-61.

77.   Lorenzi, T., et al., *Expression patterns of two serine protease HtrA1 forms in human placentas complicated by preeclampsia with and without intrauterine growth restriction.* Placenta, 2009. **30**(1): p. 35-40.

78.   Hwa, V., Y. Oh, and R.G. Rosenfeld, *The insulin-like growth factor-binding protein (IGFBP) superfamily.* Endocr Rev, 1999. **20**(6): p. 761-87.

79.   Skorko-Glonek, J., et al., *HtrA protease family as therapeutic targets.* Curr Pharm Des, 2013. **19**(6): p. 977-1009.

80.   Hasselblatt, H., et al., *Regulation of the sigmaE stress response by DegS: how the PDZ domain keeps the protease inactive in the resting state and allows integration of different OMP-derived stress signals upon folding stress.* Genes Dev, 2007. **21**(20): p. 2659-70.

81.   Oka, C., et al., *HtrA1 serine protease inhibits signaling mediated by Tgfbeta family proteins.* Development, 2004. **131**(5): p. 1041-53.

82.   Truebestein, L., et al., *Substrate-induced remodeling of the active site regulates human HTRA1 activity.* Nat Struct Mol Biol, 2011. **18**(3): p. 386-8.

83.   Vanlandewijck, M., et al., *A molecular atlas of cell types and zonation in the brain vasculature.* Nature, 2018. **554**(7693): p. 475-480.

84.   Beaufort, N., et al., *Cerebral small vessel disease-related protease HtrA1 processes latent TGF-beta binding protein 1 and facilitates TGF-beta signaling.* Proc Natl Acad Sci U S A, 2014. **111**(46): p. 16496-501.

85.	Wierer, M., et al., *Compartment-resolved Proteomic Analysis of Mouse Aorta during Atherosclerotic Plaque Formation Reveals Osteoclast-specific Protein Expression.* Mol Cell Proteomics, 2018. **17**(2): p. 321-334.

86.	Tom, I., et al., *Development of a therapeutic anti-HtrA1 antibody and the identification of DKK3 as a pharmacodynamic biomarker in geographic atrophy.* Proc Natl Acad Sci U S A, 2020. **117**(18): p. 9952-9963.

87.	Yang, Z., et al., *A variant of the HTRA1 gene increases susceptibility to age-related macular degeneration.* Science, 2006. **314**(5801): p. 992-3.

88.	Yan, Q., et al., *Genome-wide analysis of disease progression in age-related macular degeneration.* Hum Mol Genet, 2018. **27**(5): p. 929-940.

89.	Tiaden, A.N. and P.J. Richards, *The emerging roles of HTRA1 in musculoskeletal disease.* Am J Pathol, 2013. **182**(5): p. 1482-8.

90.	Baldi, A., et al., *The HtrA1 serine protease is down-regulated during human melanoma progression and represses growth of metastatic melanoma cells.* Oncogene, 2002. **21**(43): p. 6684-8.

91.	Chien, J., et al., *A candidate tumor suppressor HtrA1 is downregulated in ovarian cancer.* Oncogene, 2004. **23**(8): p. 1636-44.

92.	Altobelli, E., et al., *HtrA1: Its future potential as a novel biomarker for cancer.* Oncol Rep, 2015. **34**(2): p. 555-66.

93.	Roeben, B., et al., *Teaching NeuroImages: When alopecia and disk herniations meet vascular leukoencephalopathy: CARASIL.* Neurology, 2016. **86**(15): p. e166-e167.

94.	Uemura, M., et al., *HTRA1 Mutations Identified in Symptomatic Carriers Have the Property of Interfering the Trimer-Dependent Activation Cascade.* Front Neurol, 2019. **10**: p. 693.

95.	Howe, K.L., et al., *Ensembl 2021.* Nucleic Acids Res, 2021. **49**(D1): p. D884-D891.

96.	Sherry, S.T., et al., *dbSNP: the NCBI database of genetic variation.* Nucleic Acids Res, 2001. **29**(1): p. 308-11.

97.	Karczewski, K.J., et al., *The ExAC browser: displaying reference data information from over 60 000 exomes.* Nucleic Acids Res, 2017. **45**(D1): p. D840-D845.

98.	Karczewski, K.J., et al., *The mutational constraint spectrum quantified from variation in 141,456 humans.* Nature, 2020. **581**(7809): p. 434-443.

99.	Karczewski, K.J., et al., *Author Correction: The mutational constraint spectrum quantified from variation in 141,456 humans.* Nature, 2021. **590**(7846): p. E53.

100.	Taliun, D., et al., *Sequencing of 53,831 diverse genomes from the NHLBI TOPMed Program.* Nature, 2021. **590**(7845): p. 290-299.

101.	Adzhubei, I., D.M. Jordan, and S.R. Sunyaev, *Predicting functional effect of human missense mutations using PolyPhen-2.* Curr Protoc Hum Genet, 2013. **Chapter 7**: p. Unit7 20.

102.	Vaser, R., et al., *SIFT missense predictions for genomes.* Nat Protoc, 2016. **11**(1): p. 1-9.

103.	Schwarz, J.M., et al., *MutationTaster2: mutation prediction for the deep-sequencing age.* Nat Methods, 2014. **11**(4): p. 361-2.

104.	Choi, Y., et al., *Predicting the functional effect of amino acid substitutions and indels.* PLoS One, 2012. **7**(10): p. e46688.

105.	Reva, B., Y. Antipin, and C. Sander, *Predicting the functional impact of protein mutations: application to cancer genomics.* Nucleic Acids Res, 2011. **39**(17): p. e118.

106.	Vierkotten, S., P.S. Muether, and S. Fauser, *Overexpression of HTRA1 leads to ultrastructural changes in the elastic layer of Bruch's membrane via cleavage of extracellular matrix components.* PLoS One, 2011. **6**(8): p. e22959.

107. Pati, A.R., et al., *A new case of autosomal dominant small vessel disease carrying a novel heterozygous mutation in HTRA1 gene: 2-year follow-up.* Neurol Sci, 2018. **39**(8): p. 1479-1481.

108. Fontana, A., et al., *Probing the conformational state of apomyoglobin by limited proteolysis.* J Mol Biol, 1997. **266**(2): p. 223-30.

109. Murwantoko, et al., *Binding of proteins to the PDZ domain regulates proteolytic activity of HtrA1 serine protease.* Biochem J, 2004. **381**(Pt 3): p. 895-904.

110. Stefl, S., et al., *Molecular mechanisms of disease-causing missense mutations.* J Mol Biol, 2013. **425**(21): p. 3919-36.

111. Cartegni, L., S.L. Chew, and A.R. Krainer, *Listening to silence and understanding nonsense: exonic mutations that affect splicing.* Nat Rev Genet, 2002. **3**(4): p. 285-98.

112. Fasano, A., et al., *HTRA1 expression profile and activity on TGF-beta signaling in HTRA1 mutation carriers.* J Cell Physiol, 2020. **235**(10): p. 7120-7127.

113. Ben Jehuda, R., Y. Shemer, and O. Binah, *Genome Editing in Induced Pluripotent Stem Cells using CRISPR/Cas9.* Stem Cell Rev Rep, 2018. **14**(3): p. 323-336.

114. Mizushima, N., et al., *Autophagy fights disease through cellular self-digestion.* Nature, 2008. **451**(7182): p. 1069-75.

115. Pickart, C.M. and R.E. Cohen, *Proteasomes and their kin: proteases in the machine age.* Nat Rev Mol Cell Biol, 2004. **5**(3): p. 177-87.

116. Kiraly, O., T. Wartmann, and M. Sahin-Toth, *Missense mutations in pancreatic secretory trypsin inhibitor (SPINK1) cause intracellular retention and degradation.* Gut, 2007. **56**(10): p. 1433-8.

117. Dichgans, M., S.L. Pulit, and J. Rosand, *Stroke genetics: discovery, biology, and clinical applications.* Lancet Neurol, 2019. **18**(6): p. 587-599.

118. Goumans, M.J., Z. Liu, and P. ten Dijke, *TGF-beta signaling in vascular biology and dysfunction.* Cell Res, 2009. **19**(1): p. 116-27.

119. Jones, A., et al., *Increased expression of multifunctional serine protease, HTRA1, in retinal pigment epithelium induces polypoidal choroidal vasculopathy in mice.* Proc Natl Acad Sci U S A, 2011. **108**(35): p. 14578-83.

120. Clausen, T., et al., *HTRA proteases: regulated proteolysis in protein quality control.* Nat Rev Mol Cell Biol, 2011. **12**(3): p. 152-62.

121. Favaretto, S., et al., *A new Italian family with HTRA1 mutation associated with autosomal-dominant variant of CARASIL: Are we pointing towards a disease spectrum?* J Neurol Sci, 2019. **396**: p. 108-111.

122. Bougea, A., et al., *The first Greek case of heterozygous cerebral autosomal recessive arteriopathy with subcortical infarcts and leukoencephalopathy: An atypical clinico-radiological presentation.* Neuroradiol J, 2017. **30**(6): p. 583-585.

123. Yamashita, T., et al., *A Japanese family of autosomal dominant cerebral small vessel disease with heterozygous HTRA1 mutation showing dementia, gait disturbance and subarachnoid hemorrhage.* Vas-Cog Journal, 2018: p. 20.

124. Zhang, W.Y., F. Xie, and P.L. Lu, *Two novel heterozygous HTRA1 mutations in two pedigrees with cerebral small vessel disease families.* Neurol Sci, 2018. **39**(3): p. 497-501.

125. Zhuo, Z.L., et al., *A novel heterozygous HTRA1 mutation is associated with autosomal dominant hereditary cerebral small vessel disease.* Mol Genet Genomic Med, 2020. **8**(6): p. e1111.

126. Kono, Y., et al., *Heterozygous HTRA1 mutations with mimicking symptoms of CARASIL in two families.* Clin Neurol Neurosurg, 2018. **172**: p. 174-176.

127. Oluwole, O.J., et al., *Cerebral small vessel disease due to a unique heterozygous HTRA1 mutation in an African man.* Neurol Genet, 2020. **6**(1): p. e382.

128. Chen, Y., et al., *A novel mutation of the high-temperature requirement A serine peptidase 1 (HTRA1) gene in a Chinese family with cerebral autosomal recessive arteriopathy with subcortical infarcts and leukoencephalopathy (CARASIL).* J Int Med Res, 2013. **41**(5): p. 1445-55.

129. Ragno, M., et al., *Cutaneous Sensory and Autonomic Small Fiber Neuropathy in HTRA1-Related Cerebral Small Vessel Disease.* J Neuropathol Exp Neurol, 2020.

130. Wu, X., et al., *Heterozygous HTRA1 missense mutation in CADASIL-like family disease.* Braz J Med Biol Res, 2018. **51**(5): p. e6632.

131. Thaler, F.S., et al., *Cerebral small vessel disease caused by a novel heterozygous mutation in HTRA1.* J Neurol Sci, 2018. **388**: p. 19-21.

132. Preethish-Kumar, V., et al., *CARASIL families from India with 3 novel null mutations in the HTRA1 gene.* Neurology, 2017. **89**(23): p. 2392-2394.

133. Tateoka, T., et al., *Unusual case of cerebral small vessel disease with a heterozygous nonsense mutation in HTRA1.* J Neurol Sci, 2016. **362**: p. 144-6.

D - Acknowledgments

I would like to thank Prof. Dr. Martin Dichgans for his support and conception of this work, his scientific input and an excellent working environment at the ISD.

I would like to thank Dr. Nathalie Beaufort for her technical and educational support, great motivation and guidance through the whole project. I am very grateful to her for the helpful suggestions and constructive criticism during the preparation of this thesis.

I would like to give my appreciation to Sophie von Brauchitsch, Nicola Schieferdecker, Eva Scharrer, Andreas Zellner, Alessandro Fassano and PD Dr. Christof Haffner.

Natalie Leistner, Barbara Lindner and Manuela Schneider provided invaluable technical support.

For this thesis I received financial and educational support from the FöFoLe program of the LMU Munich.

Danke, meiner Mutter, für ihre große Geduld und liebevolle Unterstützung während meiner Ausbildung und Arbeit an dieser Dissertation.